MODELING PLASMA FLOW IN A MAGNETIC NOZZLE WITH THE LATTICE-BOLTZMANN METHOD

An Honors Fellows Thesis

by

FRANS HENDRIK EBERSOHN

Submitted to the Honors Programs Office
Texas A&M University
in partial fulfillment of the requirements for the designation as

HONORS UNDERGRADUATE RESEARCH FELLOW

April 2010

Major: Aerospace Engineering

MODELING PLASMA FLOW IN A MAGNETIC NOZZLE WITH THE LATTICE-BOLTZMANN METHOD

An Honors Fellows Thesis

by

FRANS HENDRIK EBERSOHN

Submitted to the Honors Programs Office
Texas A&M University
in partial fulfillment of the requirements for the designation as

HONORS UNDERGRADUATE RESEARCH FELLOW

Approved by:

Research Advisor: Jacques Richard
Associate Director of the Honors Programs Office: Dave A. Louis

April 2010

Major: Aerospace Engineering

ABSTRACT

Modeling Plasma Flow in a Magnetic Nozzle with the Lattice-Boltzmann Method.
(April 2010)

Frans Hendrik Ebersohn
Department of Aerospace Engineering
Texas A&M University

Research Advisor: Dr. Jacques Richard
Department of Aerospace Engineering

Magnetic nozzles must convert thermal or gyro energy of the plasma to thrust while also inducing plasma detachment in order to be effective. Plasma detachment and methods to induce plasma detachment are examined. In particular, super Alfvénic detachment and resistive detachment are examined. A parametric study of the plasma flow is conducted. Plasma flow through a magnetic nozzle is simulated using a three-dimensional, time-dependent magnetohydrodynamics (MHD) model. The MHD equations are modeled using the lattice-Boltzmann method and the linearized Boltzmann equation with the Bhatnagar-Gross-Krook operator for collisions. This thesis presents simulations of configurations and conditions related to the VASIMR propulsion scheme. This research demonstrates plasma detachment using resistive and super Alfvénic mechanisms by modeling plasma flow with the Lattice Boltzmann Method.

DEDICATION

Ek wil my eerste tesis toewy aan my ouers wie vir my alles ge gee het wat my ge bring het waar ek vandag is. Dankie vir alles en vir ewig. Daar nog baie om te kom.

ACKNOWLEDGMENTS

First and foremost I would like to thank Dr. Jacques Richard for his continued help and guidance in all of the research conducted for this thesis. I would like to thank him as well for introducing me to the subjects of plasma physics and plasma propulsion that have now captivated me.

I would also like to thank George, Karin, and Abram Ebersohn for their continued support throughout my time at Texas A&M and while working on this thesis. I would also like to thank Margeaux Horne for her help with editing and late night cups of tea.

Thank you also to the National Science Foundation for the funding given to pursue this research in the summer of 2009.

Finally I would like to thank Texas A&M University for giving me the opportunity to advance my education in Aerospace Engineering and for providing me the avenue to explore my research interests through the Undergraduate Research Fellows Program.

NOMENCLATURE

q	Electric Charge
m	Mass
I	Current
J	Current Density
ρ	Density, Charge Density
p	Pressure
ε_0	Electric Constant
μ_0	Vacuum Permeability
k	Boltzmann's Constant
r	Radial Distance
E	Electric Field
B	Magnetic Field
n	Plasma Particle Density
v,u	Velocity Components
v_A	Alfvén Velocity
r_L	Larmor Radius
τ_F	Fluid Relaxation Time
τ_B	Magnetic Field Relaxation Time
f	Probability Distribution Function
R	Universal Gas Constant

Π	Stress Term
Q	Heat Flux Term
LBE	Lattice Boltzmann Equation
LBM	Lattice Boltzmann Method
MHD	Magnetohydrodynamics
VASIMR	Variable Specific Impulse Magnetoplasma Rocket
BGK	Bhatnagar-Gross-Krook

TABLE OF CONTENTS

Page

CHAPTER Page

LIST OF FIGURES

FIGURE Page

LIST OF TABLES

CHAPTER I

INTRODUCTION

Background

Space propulsion methods are an active subject of research with many applications for future space missions. Electric propulsion and specifically plasma propulsion is of particular intrigue, with a large portion of current and future space propulsion schemes focusing on the use of plasmas. These types of propulsion when compared with conventional chemical propulsion are much more efficient with fuel, which is seen in the much higher specific impulse they have [1]. Specific impulse (I_{sp}) is a measure of the thrust generated per mass flow rate of propellant and has units of seconds. Specific impulse also compares the exit velocity of particles with the acceleration due to gravity. If a system has a high I_{sp} it produces particles with high exit velocity. Although current electric propulsion systems have higher I_{sp}, they have much lower thrust than chemical rockets. The low thrust and high I_{sp} makes electric propulsion devices suitable for long-range space missions, while chemical propulsion is used primarily for short-range missions. Current efforts, including this research, are trying to bridge the gap between high I_{sp} and high thrust systems to find a method that can produce both.

This thesis will follow the format of the *American Institute of Aeronautics and Astronautics.*

There are a variety of means to use electric and magnetic fields to manipulate plasmas for space propulsion purposes. Magnetoplasmadynamic thrusters are a specific example that utilizes the Lorentz force to produce thrust. Magnetic fields can also be used to convert the gyro motion of particles into axial motion and produce thrust as in the Variable Specific Impulse Magnetoplasma Rocket (VASIMR) [2,3]. This use of a magnetic field constitutes what is known as a magnetic nozzle. Magnetic nozzles are constructed by creating magnetic fields in which the throat has a large magnitude magnetic field that gradually lessens when moving away from the throat. Magnetic nozzles can also be used to achieve similar effects to those of physical nozzles, such as accelerating flows to supersonic speeds through a converging diverging section [4]. Research in fusion involving plasmas may also be adapted for propulsion uses and would require the use of magnetic nozzles. Many currently researched space propulsion methods may employ magnetic nozzles as part of the propulsion system, thus researching these nozzles is of prime importance.

Effective magnetic nozzles are defined by a variety of factors. One measure of this is the ability of the magnetic nozzle to convert or directionalize either thermal energy or gyro motion into thrust. Plasma detachment is also necessary so that the plasma will break free from the applied magnetic field and produce thrust. A variety of possible scenarios have been conceived to achieve this detachment and some of these are examined in this thesis.

Developing a computational model for studying the behavior of plasma flowing through a magnetic nozzle is an active part of plasma propulsion research. Computational models have a distinct advantage over physical tests in that they cost a great deal less and can be performed many more times while providing results similar to what would be seen in physical experiments. Creating a model that correctly predicts plasma behavior can thus greatly further the research being performed on these topics and expand the understanding of the physics involved in these systems. A well-developed computational model can be used in designing systems that employ magnetic nozzles or for modeling behavior of laboratory plasmas. A number of models currently exist, each making certain assumptions and having certain limitations, leaving a gap for more research to be conducted.

In the research this paper presents, a computational model is used to predict the behavior of plasma in a magnetic nozzle. The model is a modified from previous versions to further model magnetic nozzles and is verified with work conducted by similar projects on VASIMR and other plasma flow analyses [5,6,7,8]. The computational model is based on the lattice Boltzmann Method (LBM), which is based on kinetic theory [9,10,11]. The LBM is used to obtain the Navier-Stokes equations and uses the Bhatnagar-Gross-Krook collision operator to model collisions [9,10,11]. This is also used to solve the MHD equations from kinetic theory [12]. The limitations of this current model are low Mach number and incompressibility.

Objectives of thesis

This thesis strives to achieve certain objectives. The first of these is to model the physics of the plasma correctly using the governing Navier Stokes and magnetohydrodynamic equations. A parametric study will achieve these objectives by:

- Qualitatively showing that plasma flow behaves as expected with variation of key parameters (to be identified) that are characteristics of the plasma
- Qualitatively showing that the plasma flow behaves as expected when subjected to different magnetic fields (verification of the physics)

Validation of the results reported by the computational model will also be sought through the following areas:

- Correctly modeling real world systems currently in use
- Matching results of other computational methods

The specific study of magnetic nozzles will attempt to achieve the following objectives:

- Detachment of the plasma from the applied magnetic field
- Discussion of detachment mechanisms at work

Contributions from this research will be in the following areas:

- Space Propulsion
- MHD-LBM Modeling and Validation
- Magnetic nozzle research

Thesis outline

Following the introduction there is a literature review section discussing previous work which has been conducted on this subject. This is followed by a theory section covering the main physics involved. After this, there is a section discussing the computational model used to model the plasma flow. A results section follows this and presents the key results of the thesis. The conclusion closes the thesis by highlighting and discussing the main results of the research. Possible future work is also discussed in the conclusion.

CHAPTER II

LITERATURE REVIEW

Magnetic nozzles are an active subject of research that also has a strong foundation in past research. Research in magnetic nozzles has increased in the last few years due to the interest developing in fusion based propulsion systems such as the Variable Specific Impulse Magnetoplasma Rocket (VASIMR), seen in Figure 1, and the Laser Fusion Rocket (LFR). VASIMR uses radio waves to ionize and heat the plasma, which then expands through the magnetic nozzle to create thrust [2,3].

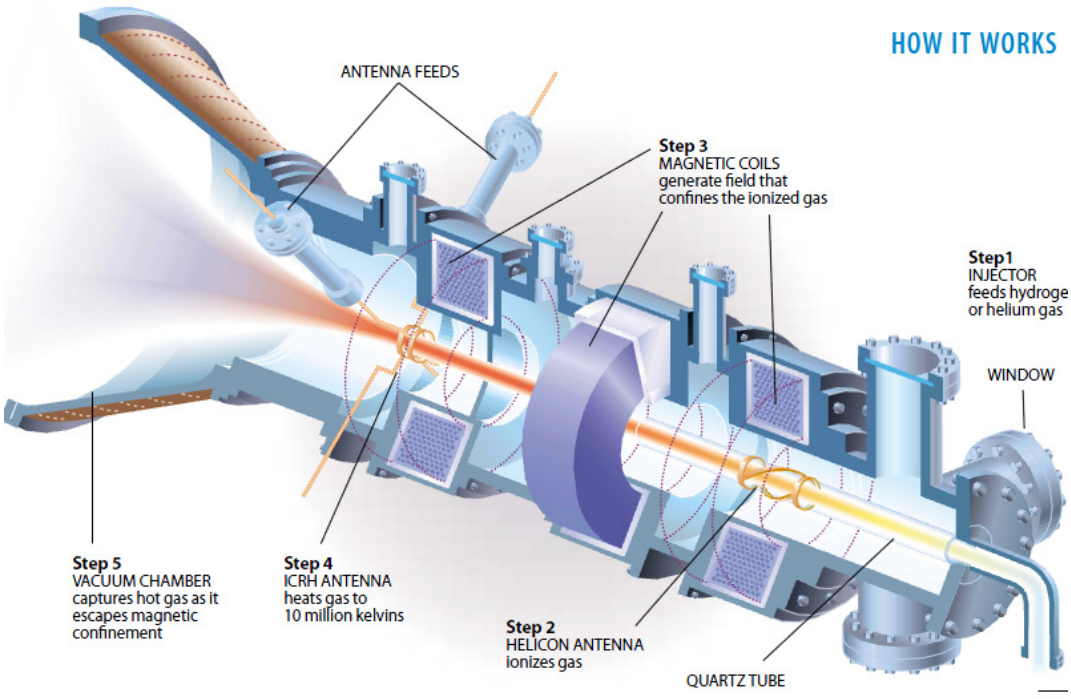

Figure 1. VASIMR schematic [2]

The LFR uses magnetic fields to compress expansion of plasmas in a fusion reaction [13].

The research on magnetic nozzles is in three main categories, modeling of the plasma through computational methods, theoretical work on the physics of magnetic nozzles, and real world testing of magnetic nozzles. The purpose of my research is to model magnetic nozzles, validate the correct physics in the model, and demonstrate effectivedetachment; thus a strong background of relatable research is required. Plasma detachment in the VASIMR system has been modelled in a variety of ways. In particular the company developing VASIMR, Ad Astra, has perfomed modeling. Plasma detachment in VASIMR is postulated to be achieved by reaching super-Alfvénic flows which are characterized when the ratio β is above unity. The physics behind this will be explained in the next chapter. The domain for this modelling consists of the "aft end-cell" and begins at the inlet of the exhaust at $z = 1$ as seen in Figure 2. In Figure 2 the magnetic field lines for VASIMR are shown as well as the strength of the magnetic field while progressing axially. The plasma is ionized in the forward region, is then energized in the central region by Ion-Cyclotron Resonant Frequency heating, and is finally expanded out in the aft region by the magnetic nozzle.

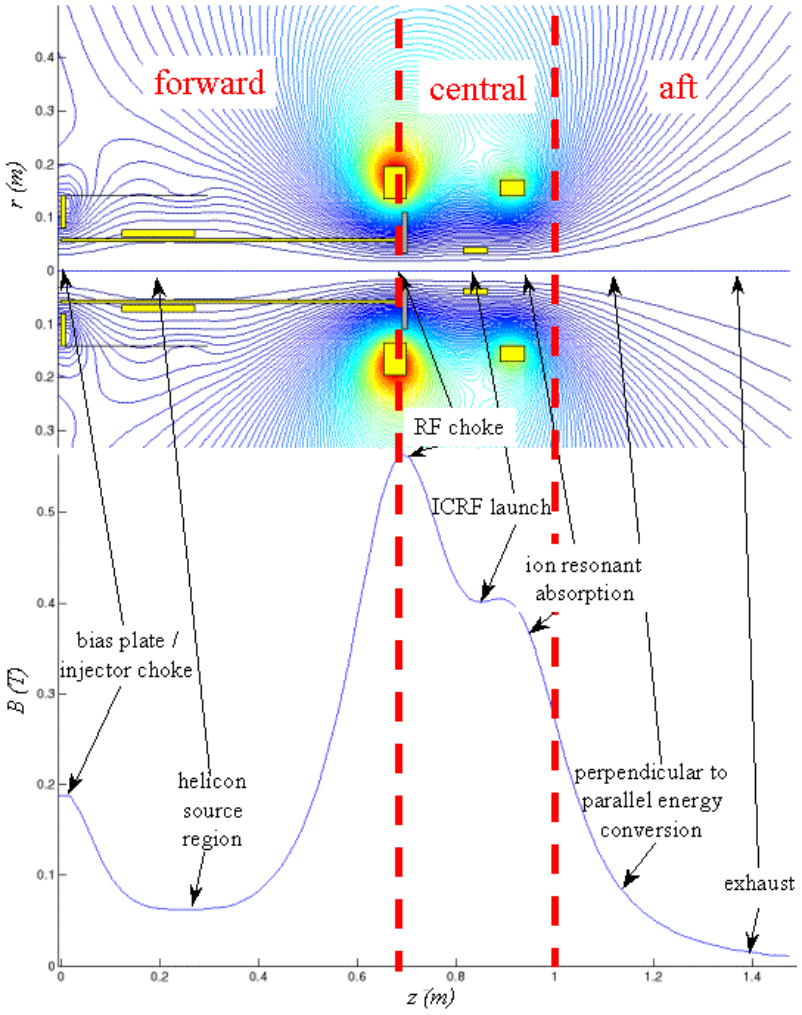

Figure 2. Geometry and magnetic field configuration for VASIMR thruster [14]

Both a particle trajectory method and MHD code were used to model the flow. The results from these methods were then compared with one another. A variety of operational parameters are given which may be used to model similar flow for validation. Figure 3 shows the typical ion trajectory, axial and perpendicular energies, and the magnetic moment found by the particle trajectory method.

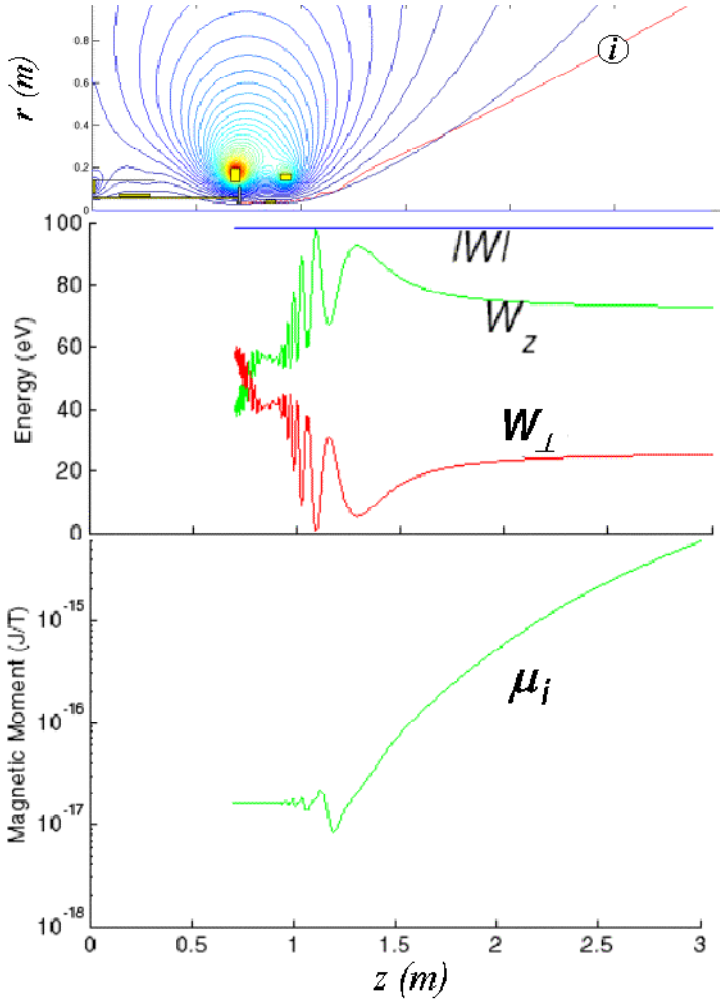

Figure 3. Top: Magnetic field lines and test ion trajectory in VASIMR. Middle: Total, axial, and perpendicular energies of ion. Bottom: Magnetic moment [14]

Through the particle simulations certain indications were found that demostrated plasma detachment. The conditions of particular interest are:

1. Axial ion energy approaches a constant value

2. Magnetic moment increases
3. The plasma β is greater than unity

A 2-D MHD simulation using the Non-Ideal Magnetohydrodynamics with Rotation, Open Discussion (NIMROD) code [14] was also performed yielding similar results. Figure 4 shows the relationship between the results of the two models, the MHD method and the particle simulation method. This model has since been changed into a three dimensional model and is currently being used to study the plasma parameters and detachment process of plasma from the VASIMR engine. The goal of its use is to optimize the design in terms of nozzle efficiency, plasma detachment, and stability of the plasma flow.

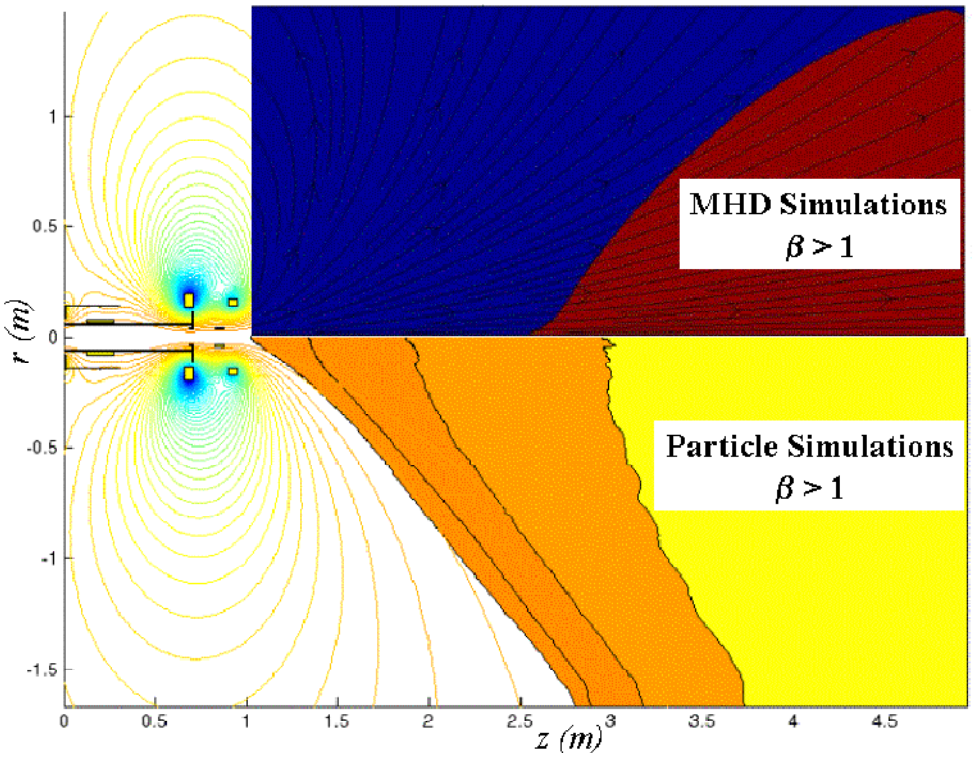

Figure 4. 2D picture of plasma beta in VASIMR with magnetic field lines [14]

Currently a three dimensional MHD code called MACH3, an updated version of the MACH2 code, is also being used to model plasma flow. MACH3 is a time-dependent, non-ideal MHD, arbitrary Lagrangian-Eulerian (ALE) code [4]. Results from this code can be used for validation purposes, some of which are shown in Figure 5. This figure shows a magnetic nozzle acting much like a conventional converging-diverging nozzle. The simulations for this code incorporated a current layer around the plasma. Research being conducted using this code does not specifically examine plasma detachment from the magnetic field.

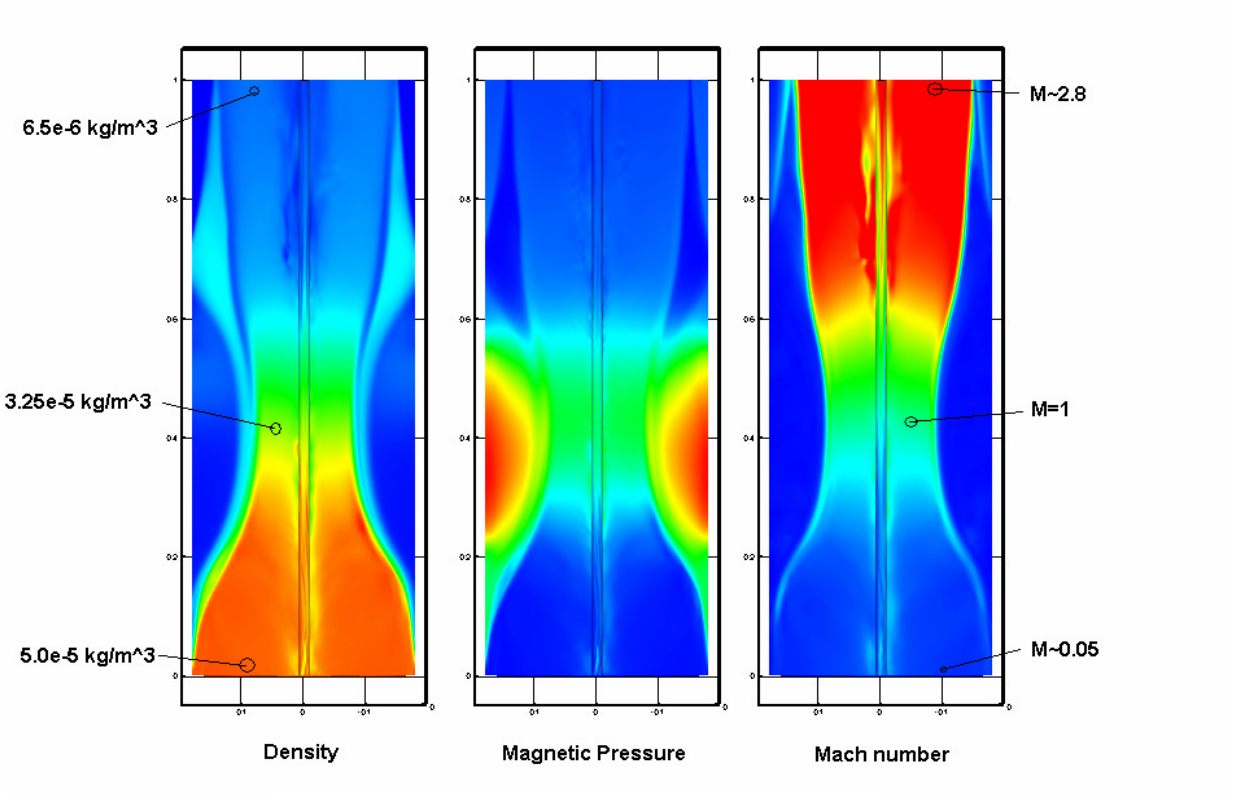

Figure 5. Density, magnetic pressure, and Mach number profiles [4]

Research is also being conducted using a 2D3V electromagnetic fully Particle-In-Cell (TRISTAN) code to study the behavior of plasma in a magnetic nozzle [15]. This code is being used in conjunction with the LFR research and examines methods for achieving plasma detachment. The configuration of these tests can be seen in Figure 6 along with the ion positions at a steady state time step in Figure 7.

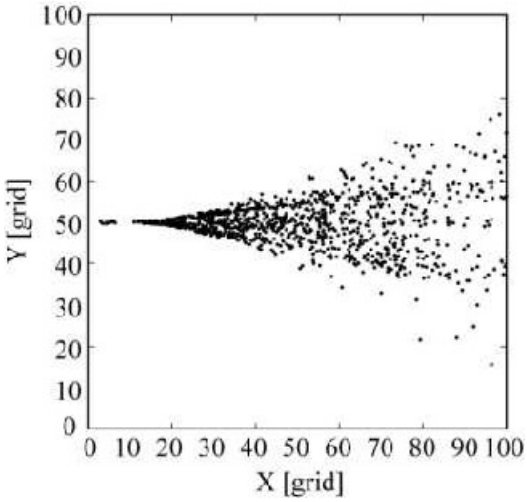

Figure 6. Schematic calculation model for TRISTAN [15]

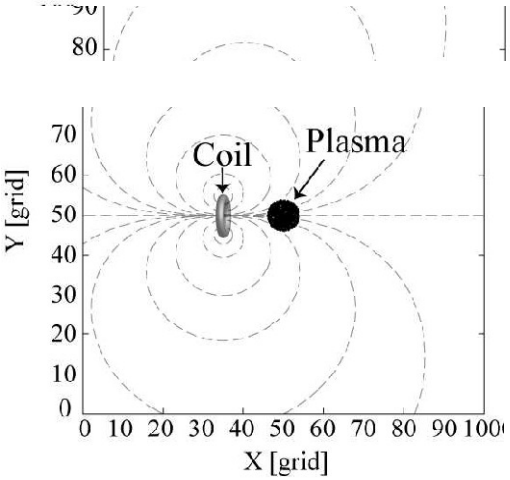

Figure 7. Position of ions from TRISTAN [15]

Older research on magnetic nozzles focused more on the use of magnetic nozzles in non-fusion based propulsion systems. Research by Hoyt focused on coaxial thrusters and finding efficient detachment of the plasma from the magnetic field lines. The MACH2 code was used for this modeling and is a 2 ½ dimensional resistive MHD code including the Hall effect. The use of trim coils to adjust the magnetic field to induce detachment was also examined. Trim coils are current loops that get gradually larger or reduce in current when moving away from the throat of the nozzle. Based on the research in these papers, using trim coils to should improve the detachment of the plasma [16,17].

Research has been performed to determine the necessary conditions for plasma to detach from a magnetic nozzle. In particular, the use of super-Alfvénic flow to detach from the magnetic field lines is examined. It has been shown that slowly diverging nozzles

provide a well-controlled transition to super-Alfvénic flow in the plasma [18]. This particular research incorporated a perfectly conducting, axisymmetric wall to confine a given magnetic flux. The efficiency of the magnetic nozzle was also examined. The nozzle efficiency measures the ratio of the momentum flux of the incoming flow with that of the outgoing flow.

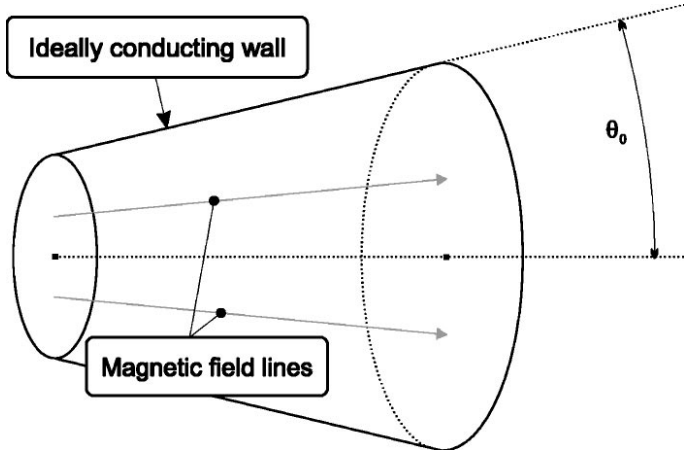

Figure 8. Magnetic nozzle with conducting wall of divergence angle θ_0 [18]

This research was then expanded into doing modeling of steady state flow through a magnetic nozzle [19]. A Lagrangian code incorporating kinetic treatment was used simulate the plasma flow and analyze the detachment of the plasma. For all of the cases ran by this experiment supersonic but sub-Alfvénic flow was used for the incoming flow so that effects associated with ambipolar electric fields and electron pressures can be neglected. A benchmark case was run incorporating a conducting wall to confirm their previous theoretical study. Cases were also run with a cylindrical nozzle with no

conducting wall and a vacuum gap between the plasma and the nozzle wall. For this configuration cases were ran with an inlet velocity that was only axial and also with an inlet velocity with gyro motion. Both of these types of cases demonstrated detachment from the magnetic field lines as well as the gyro motion case showing conversion of gyro motion to axial motion. Figure 9 shows graphs of both of these cases. An additional simulation was also run to mimic the results of the Detachment Demonstration Experiment run by NASA. The code was shown to predict accurately the physics of the experiment.

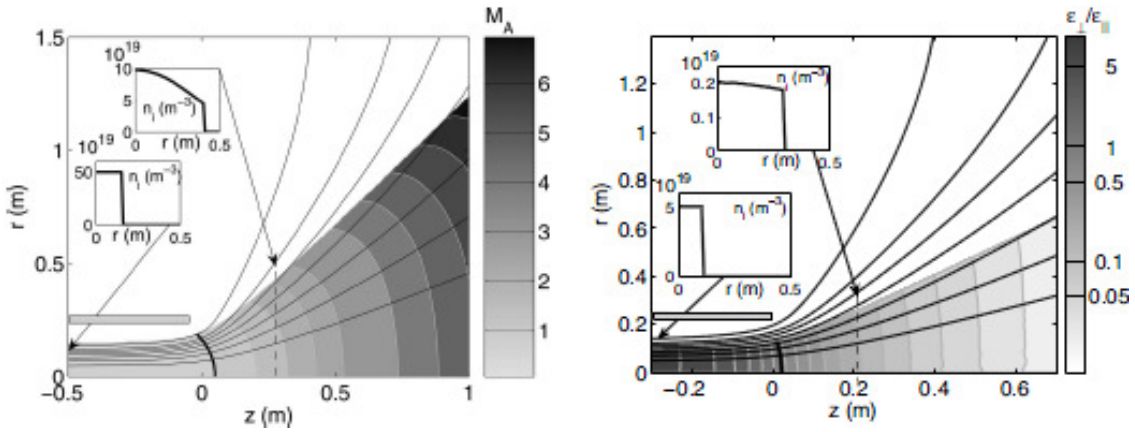

Figure 9. Left: Sub- to super-Alfvénic transition in plume of cylindrical nozzle. Light gray bar is solenoid. Right: Transition from sub- to super-Alfvénic flow with a conversion of gyroenergy [19]

Another study [20] conducted research with both computational and experimental studies. From their experimental studies they gained a variety radial density profiles at various axial positions in the testing device. Simulations with cross-field diffusion and

super-Alfvénic detachment were found to help explain the found profiles. It was also found that after particles reach β greater than unity they will follow ballistic trajectories. Figure 10 shows results found from this study of the electron inertia detachment with a gradient of the parameter G characterizing this detachment. Magnetic field lines are also shown.

A general study of magnetic nozzles and detachment methods, including a MHD simulation method has also been conducted [21,22]. Five specific models of detachment are discussed. These models are:

1. Resistive Detachment
2. Kinetic Detachment
3. Recombination Detachment
4. Non-Adiabatic Detachment
5. Electron Inertia Detachment

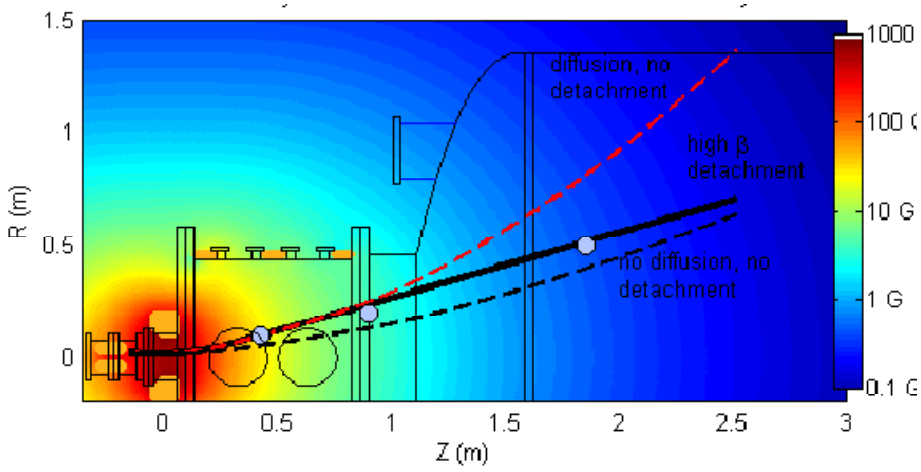

Figure 10. Plume trajectory for helium. Lines show magnetic field lines [20]

Of these methods only the first two can be examined by continuum simulation models [21,22]. Particle in cell methods must be used to examine the other three scenarios for detachment. Plasma detachment by achieving super-Alfvénic speeds was found in the simulations with Alfvén Mach number profiles. This detachment is postulated to be caused by large azimuthal currents.

In conclusion there are a variety of magnetic nozzle studies currently being performed as well as past research which can be used for validation and giving insight on achieving correct, effective detachment. Results will be compared to both theory and analytical results to determine the validity of the LBM plasma modeling.

CHAPTER III

THEORY

Electromagnetism

Electromagnetism is a branch of physics which focuses on the interactions between charges, electric fields, and magnetic fields. The basis of the idea of charge is that an object or particle can possess or gain a charge that is either positive or negative. The interactions of charges are brought about by the positive charge of protons and the negative charge of electrons and are responsible for nearly everything in chemistry. Two objects with the same charge repel each other, while two objects with different charges attract one another. This attraction is characterized by a force between the particles defined by Coulomb's Law.

$$\vec{F} = \frac{1}{4\pi\varepsilon_0}\frac{q_1 q_2}{r^2}\hat{r} \tag{3.1}$$

From this force the concept of the electric field is developed. The equation for an electric field is the same as Coulomb's Law except that one of the charges is removed.

$$\vec{E} = \frac{1}{4\pi\varepsilon_0}\frac{q}{r^2}\hat{r} \tag{3.2}$$

The electric field describes what forces a charged particle can experience in the presence of another charged particle or group of charged particles. From the equation of an electric field the electric potential can also be developed. The electric potential is the integral of the electric field over an arbitrary path.

$$\varphi_E = \int_C \vec{E} \cdot d\vec{l} \tag{3.3}$$

The electric potential can be used to find the potential energy by multiplying by the charge q.

$$U_E = q\varphi_E \tag{3.4}$$

An electric current is defined as the movement of charges through a medium. Sign convention shows that positive charges are moving through the medium but in fact the negative charges in the form of electrons are often what are in fact in motion. This movement can be caused by electric fields or by differences in electric potential. When charge moves through a medium, such as a wire, it can also create what is known as a magnetic field. In Figure 11 current flows in the z direction by positive charges moving in that direction.

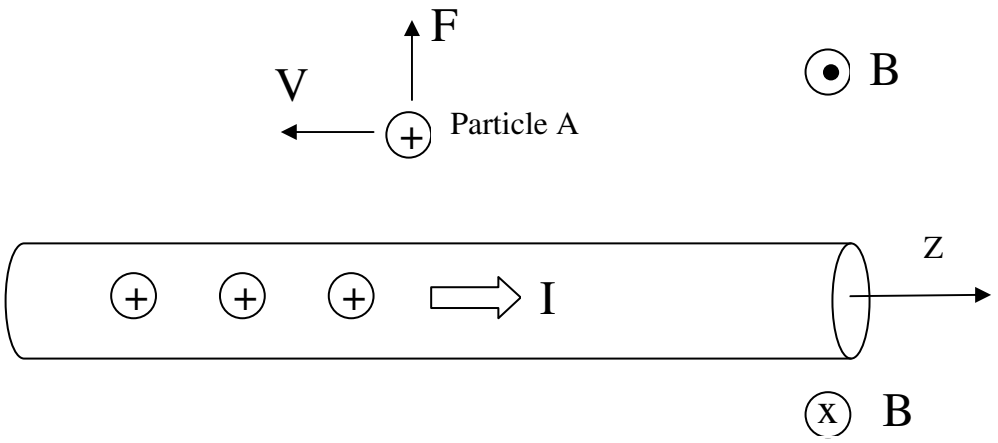

Figure 11. Current carrying wire magnetic field

There is also a positively charged Particle A some distance away from this wire. If Particle A has no velocity it experiences no force because an equal amount of positive charges are flowing in the wire in the z direction as negative charges moving in the negative z direction. This is the nature of current in that positive and negative charges flow in opposite directions to produce current. However, if Particle A moves in the negative z direction as pictured it sees more positive charges than negative charges and experiences a force in the radial direction away from the wire. Thinking of relative velocities, Particle A will see the flowing positive charges passing at a rate equal to the velocity of the flowing charge plus the velocity of Particle A. However, Particle A only sees the negative flowing charges at a velocity equal to the difference between the velocities of the negative flowing charges and Particle A. To define this force the current is said to create a magnetic field which is shown in the figure as B with direction out of the page above the wire and into the page below the wire. The direction of the magnetic field is defined so that the force on the particle is equal to the following equation known as the Biot-Savart Law:

$$\vec{B} = \int \frac{\mu_0}{4\pi} \frac{Idl \times \hat{r}}{r^2} \tag{3.5}$$

The combination of magnetic and electric field effects on a particle defines the Lorentz Force equation shown below, which incorporates the forces on a particle by an electric and magnetic field.

$$\vec{F} = q\left(\vec{E} + \vec{v} \times \vec{B}\right) \tag{3.6}$$

In general charged particles will revolve around magnetic field lines due to the Lorentz Force.

Altogether most of electromagnetism is defined by a set of equations known as Maxwell's equations which describe the relationship between charge, electric fields, and magnetic fields. These equations are given below:

$$\nabla \cdot \vec{E} = \frac{\rho}{\varepsilon_0} \tag{3.7}$$

$$\nabla \cdot \vec{B} = 0 \tag{3.8}$$

$$\nabla \times \vec{E} = \frac{\partial \vec{B}}{\partial t} \tag{3.9}$$

$$\nabla \times \vec{B} = \mu_0 \vec{J} + \mu_0 \varepsilon_0 \frac{\partial \vec{E}}{\partial t} \tag{3.10}$$

Kinetic plasma theory and Boltzmann equation

There are three different levels used to describe the behavior of gasses. To see the difference between these the Knudsen number is used in which L is the characteristic length and λ is the mean free path.

$$Kn = \frac{\lambda}{L} \tag{3.11}$$

The first of these levels is the microscopic level and focuses on individual particle behavior. The motion at this level is governed by Newtonian physics. This method of

describing the behavior of gases is called Molecular Dynamics and while being the most accurate, is only viable for a small number of particles due to its complexity.

Another level is the macroscopic level that examines the behavior of a large amount of particles together in what is known as a continuum. This level is described primarily by the Euler and Navier-Stokes equations and is defined by Knudsen numbers less than .2. At the macroscopic level, intuition about the behavior of gasses is useful as it is the level people are most familiar with. Macroscopic properties such as pressure, viscosity, and temperature all arise from molecular behavior and collisions.

The final level which can be used to describe the behavior of a gas is the mesoscopic level. This level falls between the microscopic and macroscopic levels and is governed by kinetic theory. This level can describe Knudsen numbers from 0 to 100. Kinetic theory is defined by using probability to model a fluid. Statistical mechanics describes the fluid flow, is defined by kinetic theory, and is governed by the Boltzmann Equation shown below where the collision term on the right-hand side is the Boltzmann collision integral [5,6].

$$\frac{\partial f_\alpha}{\partial t} + \vec{c} \cdot \nabla f_\alpha + \vec{a} \cdot \nabla_c f_\alpha = \left.\frac{\partial f}{\partial t}\right|_{coll} \tag{3.12}$$

In the Boltzmann equation the function f is the probability distribution function which gives the probability of a particle being at a certain velocity in a gas. The concept of velocity space is also introduced by the Boltzmann equation and the function f

corresponds to the equivalent of density in 6-D space. The probability function used for this study is the Maxwellian distribution [23].

$$f(v_i) = \left(\frac{m}{2\pi kT}\right)^{3/2} e^{\left(-\frac{m}{2kT}\left(v_1^2+v_2^2+v_3^2\right)\right)} \tag{3.13}$$

From the Maxwellian distribution the most probable, average, and root-mean-square molecular speed are defined.

$$v_{m,p} = \sqrt{2RT} \tag{3.14}$$

$$\overline{v} = \sqrt{\frac{8RT}{\pi}} \tag{3.15}$$

$$v_{rms} = \sqrt{3RT} \tag{3.16}$$

The most probable speed, $v_{m,p}$, is at the maximum of the Maxwell distribution, the average speed is a weighted average of all of the speeds in the distribution, and the root mean square speed, v_{rms}, is related to the kinetic energy and is the square root of the velocity squared average.

A variety of assumptions are made in developing the Boltzmann equation [6]:

- The number of particles is very large
- The mass of individual particles is small compared to the mass of the system
- The range of intermolecular forces is small so that the mean free path is finite and constant

The Boltzmann equation is used to describe the effects on the probability function by a variety of influences. The collisional term in the Boltzmann equation can be modeled

using a linear collision operator known as the Bhatnagar-Gross-Krook collision model [6].

$$\left.\frac{\partial f}{\partial t}\right|_{coll} = -\frac{1}{\tau_f}\left(f_\alpha - f_\alpha^{eq}\right) \tag{3.17}$$

The Boltzmann equation can be used to satisfy conservation of mass, momentum, and energy for the mesoscopic level. Using the Boltzmann equation, the zeroth moment develops continuity, the first moment develops conservation of momentum, and the second moment develops conservation of energy. Macroscopic properties can also be found by integrating the probability function over the velocity space. The first moment equation can be used to get the Navier-Stokes equations used at the continuum level.

Plasma physics

Plasmas are a state of matter that makes up approximately 99 percent of the universe. Though people do not regularly interact with plasmas, they are present here on Earth and are abundant in the universe. The Aurora Borealis and the sun are examples of plasmas on our planet and in our solar system. Plasmas are defined as quasineutral gases made of both neutral and charged particles that have collective behavior. They are also known as the fourth state of matter and can be described as ionized gases in which the negatively charged electrons have separated from the atoms leaving positively charged ions. This separation of particles produces free ions and electrons, creating unique electromagnetic properties in the plasma. Plasma propulsion manipulates these plasmas and their

electromagnetic properties with magnetic and electric fields to produce thrust for the use of spacecraft [23].

Plasmas occur primarily due to extremely high temperatures. Some laboratory plasmas have temperatures around one million Kelvin and have densities of about 10^{18} particles per meter cubed. Though they may be at high temperatures, only few collide with a surface and transfer heat to it. It is also of note that the electrons and ions can have separate temperatures [23].

Temperature in gases is primarily defined by the kinetic energy of the particles in the gas. A gas however does not have all particles at the same velocity, instead a gas at thermal equilibrium has particles of varying velocities with the Maxwell distribution being the most probable distribution of these velocities. This variation of velocities creates what is known as velocity space. The Maxwellian distribution function, shown below, for one dimension when integrated over all velocities gives the number of particles per unit volume [23].

$$f(u) = A\exp\left(\frac{-\frac{1}{2}mu^2}{KT}\right) \tag{3.18}$$

In this equation A is a constant, m is mass, u is velocity, K is the Boltzmann's constant, and T is the temperature. Manipulating this equation allows for the calculation of various properties in the plasma. For example average kinetic energy is calculated by

the following equation when integrating over the entire velocity space from negative to positive infinity [23].

$$E_{av} = \frac{\int_{-\infty}^{\infty} \frac{1}{2} m u^2 f(u) du}{\int_{-\infty}^{\infty} f(u) du} \tag{3.19}$$

The definition for plasmas states that they are quasineutral and have collective behavior. Quasineutrality implies that when concentrations of charge or external potentials arise in plasma, they are shielded out in a length much smaller than the system dimension. This results from a phenomenon known as Debye shielding. Quasineutrality also leads to the assumption that the ion and electron densities are equal and have a common density known as the plasma density, n. The term collective behavior implies that there are enough particles so that shielding can occur. These two definition help define two of the conditions for an ionized gas to be a plasma. There is also a third condition which states that the interactions in plasma must be controlled by electromagnetic forces rather than hydrostatic forces. This third condition is defined by requiring the plasma oscillation frequency to be greater than the frequency of collisions [23].

The motion of particles in plasma is defined by the electromagnetic effects that the ions and electrons have on one another as well as the effects of outside fields. In particular when under the influence of a magnetic field the charged particles will revolve around

the magnetic field lines. This is caused by the Lorentz Force and is characterized by the cyclotron frequency and the Larmor radius [23].

$$\omega_c = \frac{|q|B}{m} \tag{3.20}$$

$$r_L = \frac{v_\perp}{\omega_c} \tag{3.21}$$

Looking at these equations it can be seen that by the electrons having smaller mass, they have much higher cyclotron frequencies and much smaller Larmor radii under the same conditions as the ions. [23].

Another important parameter of plasmas is the plasma frequency which is related to the oscillation of electron density in plasmas.

$$\omega_{pe} = \sqrt{\frac{n_0 q_e}{\varepsilon_0 m_e}} \tag{3.22}$$

Collisions in plasmas are more complex than in regular fluids due to the effect of the long range electromagnetic forces. In particular the collisions can be modeled in various ways, two of which are the Fokker-Planck Collision Operator and the BGK Collision Operator.

Kinetic plasma theory and magnetohydrodynamics

Kinetic plasma theory is the branch of kinetic theory that is of particular interest. As previously mentioned there are three scales of looking at the behavior of plasmas which result in three methods to model plasmas, the single particle method, the kinetic theory

method, and the continuum method. Kinetic plasma theory utilizes the Boltzmann equation to describe the collective behavior of charged particles. A new Boltzmann equation for plasmas is shown below which includes the Lorentz force term to account for the long distance forces from electromagnetism [6].

$$\frac{\partial f_\alpha}{\partial t} + \vec{v} \cdot \frac{\partial f_\alpha}{\partial r} + \frac{q_\alpha}{m_\alpha}(\vec{E} + \vec{v} \times \vec{B}) \cdot \frac{\partial f_\alpha}{\partial \vec{v}} = \left.\frac{\partial f}{\partial t}\right|_{coll} \tag{3.23}$$

Using this Boltzmann equation and integrating the zeroth, first, and second moments over the velocity space yields the new continuity, conservation of momentum, and conservation of energy equations. To complete these equations additional terms involved in electromagnetic and particles collisions are also included. The definitions of pressure and temperature along with substitution for collisional terms lead to new equations for momentum and energy [6].

$$\frac{\partial n_\alpha}{\partial t} + \nabla \cdot (n_\alpha \vec{u}_\alpha) = 0 \tag{3.24}$$

$$\frac{\partial}{\partial t}(n_\alpha m_\alpha \vec{u}_\alpha) + \vec{u}_\alpha \nabla \cdot (n_\alpha m_\alpha \vec{u}_\alpha) = -\nabla \cdot p_\alpha - q_\alpha n_\alpha (\vec{E} + \vec{u}_\alpha \times \vec{B}) - \nabla \cdot \Pi_\alpha + \vec{R}_\alpha \tag{3.25}$$

$$\frac{3}{2}\frac{\partial}{\partial t}(n_\alpha k T_\alpha) + \frac{3}{2}\vec{u}_\alpha \cdot \nabla(n_\alpha k T_\alpha) + n_\alpha k T_\alpha \nabla \cdot \vec{u}_\alpha = -\Pi_\alpha : \nabla \vec{u}_\alpha - \nabla \cdot \vec{h}_\alpha + Q_\alpha \tag{3.26}$$

These equations are split up into two fluid equations to model plasma consisting of electrons and a single type of ion separately.

The Magnetohydrodynamic (MHD) equations are derived from these fluid equations and incorporate macroscopic length scale assumptions. Magnetohydrodynamics is used to

study the dynamics of electrically conducting fluids and incorporates a combination of Maxwell's equations and the Navier-Stokes Equations. Among the assumptions made for the MHD equations are those previously mentioned in the plasma physics section. The summations of the two fluid equations create the one-fluid macroscopic equations [6].

$$\rho = n_e m_e + n_i m_i \tag{3.27}$$

$$\rho_0 = q_e n_e + q_i n_i \tag{3.28}$$

$$\vec{j} = n_e q_e \vec{u}_e + n_i q_i \vec{u}_i \tag{3.29}$$

$$\rho\vec{v} = n_e m_e \vec{u}_e + n_i m_i \vec{u}_i \tag{3.30}$$

$$p = p_e + p_i \tag{3.31}$$

At the macroscopic level the stress and heat flux terms are redefined to terms more similar to the Navier-Stokes equations. Using continuity, the newly found conservation of momentum, the magnetic induction equation, and Maxwell's third equations leads finally to the MHD equations which work together to describe a magnetized flow in an induced magnetic field [6].

$$\frac{\partial \rho}{\partial t} + \nabla \cdot \left(\rho \vec{v}\right) = 0 \tag{3.32}$$

$$\frac{\partial \rho \vec{v}}{\partial t} + \vec{v} \cdot \nabla \rho \vec{v} = -\nabla p - \nabla\left(\frac{B^2}{2\mu_0}\right) + \frac{1}{\mu_0}\left(\vec{B} \cdot \nabla\right)\vec{B} + \mu \nabla^2 \vec{v} \tag{3.33}$$

$$\frac{\partial \vec{B}}{\partial t} + \vec{v} \cdot \nabla \vec{B} = \vec{B} \cdot \nabla \vec{v} + \frac{\eta}{\mu_0} \nabla^2 \vec{B} \tag{3.34}$$

$$\nabla \cdot \vec{B} = 0 \tag{3.35}$$

When using the MHD equations certain characteristic parameters are used to analyze the behavior of the flow. The Reynolds number and the Magnetic Reynolds number are quantities that compare the convective to the diffusive behavior of the fluid. Both of these are used to analyze the specific behavior of a fluid. The Reynolds number deals with the viscous forces in a fluid while the Magnetic Reynolds number deals with the diffusivity. The Reynolds number and the magnetic Reynolds number are inversely proportional to the fluid's relaxation time and magnetic relaxation time respectively. Thus, they are also inversely proportional to viscosity and magnetic diffusivity respectively.

$$R_e = \frac{\rho v L}{\mu} \tag{3.36}$$

$$\tau_f \propto \mu \tag{3.37}$$

$$R_m = \frac{\mu_0 v L}{\eta} \tag{3.38}$$

$$\tau_B \propto \eta \tag{3.39}$$

The relaxation time of a fluid and a magnetic field is the time it takes to return to equilibrium after a disturbance has been removed. This relaxation time is inversely proportional to collision frequency and is directly proportional to the diffusive behavior of the plasma.

The interaction parameter can also be used to determine the characteristics of plasma by comparing the Lorentz force to the inertial force and is important for looking at vorticity

and turbulence. Another parameter that can be used is the Hartmann number which compares the Lorentz force to the viscous force and is important in boundary layer analysis under the effects of magnetic fields [6].

$$N = \frac{\sigma B^2 l}{\rho u} \tag{3.40}$$

$$H = \frac{B_0 L}{\sqrt{\rho_0 \eta \nu}} \tag{3.41}$$

Plasma detachment mechanics

Magnetic nozzles must accelerate plasma to high velocities while also inducing detachment of the plasma particles from the applied magnetic field. If detachment does not occur the particles will follow the field lines back to the craft and no thrust will be gained. Among the methods that can be used are those which maintain the "frozen-in" condition by the plasma detaching along with the magnetic field lines being stretched [18]. Detachment can also be caused by breaking the "frozen-in" condition . Among the currently examined methods to induce detachment are shown below [20,21].

1. Resistive Detachment
2. Kinetic Detachment
3. Recombination Detachment
4. Non-Adiabatic Detachment
5. Electron Inertia Detachment

Resistive detachment can occur when plasma conductivity is low and collisions can cause motion perpendicular to the magnetic field lines. These collisions are caused by

the Coulomb force between ions and electrons or by the interactions between electrons and electromagnetic waves. This method of detachment was analyzed by Hooper [24] and showed that the transport across magnetic field lines could lead to a loss of magnetic flux over time and violating the "frozen-in" condition guaranteed by Maxwell's equations. This loss was characterized by the following equation.

$$\frac{\psi(t)}{\psi(0)} \propto \exp\left(-\int\left(\frac{\varepsilon_0 \eta \omega_p}{u}\right)dl\right) \propto \exp\left(-\int\left(\frac{\nu_{coll}}{u}\right)dl\right) \tag{3.42}$$

Resistive detachment was also examined by Moses [25] who showed that this detachment is caused by the plasma having a finite resistivity which causes diffusion of the plasma and separation from the magnetic field lines. Having an exceedingly resistive plasma however also limits the positive effects that the magnetic field can have on the plasma flow.

Kinetic detachment occurs when the flow velocity exceeds what is known as the Alfvén speed. The Alfvén speed is the speed at which hydromagnetic waves travel along a magnetic field line and is the characteristic speed at which perturbations of magnetic field lines travel [23].

$$v_A = \frac{B}{\sqrt{\mu_0 \rho}} \tag{3.43}$$

Thus the Alfvén speed is very similar to the speed of sound in regular fluids and when exceeded perturbations in the magnetic field do not propagate upstream. By the fluid exceeding the Alfvén speed, the kinetic energy of the plasma exceeds the magnetic field

energy. The ratios of these two energies are seen in the quantities β and the Alfvén Mach.

$$\beta = \frac{\left(\frac{\rho u^2}{2}\right)}{\left(\frac{B^2}{2\mu_0}\right)} = \left(\frac{u}{v_A}\right)^2 = M_A{}^2 \tag{3.44}$$

When the Alfvén Mach or β exceed unity, detachment occurs by there being enough kinetic energy to tear away from the magnetic field lines. This condition can occur as the plasma expands in a magnetic nozzle where the magnetic field strength is decreases, the plasma velocity increases, and the β is increasing. A study was conducted for collision-less detachment with a conical conducting wall that shows that this is an effective means of detachment and predicted detachment efficiency according to the following equation [18].

$$\eta \approx 1 - \frac{\theta_0^2}{4} - \frac{v_A}{2v^2} \tag{3.45}$$

Recombination detachment is achieved by recombining ions with electrons in the plasma to produce neutrals. These neutrals can then escape and detach from the field lines. To achieve this sufficient recombination rates are necessary, which is the difficulty in achieving this form of detachment.

Non-Adiabatic detachment involves breaking the condition of the invariance of a charged particle's magnetic moment by having magnetic fields that have strong spatial variation. By breaking this adiabatic invariant, the particles are no longer confined to

travel along the magnetic field lines and can detach. The breaking of this condition can occur when the ratio of the Larmor radius of the particle to the length scale of change for the magnetic field is greater than unity. This ratio could be greater than unity for ions, which have much larger Larmor radii than electrons, but is typically not close to unity for electrons and they will remain trapped. This method thus has a problem by not preserving quisineutrality [24].

Electron inertia detachment proposes that electrons can cause collision-less detachment by inhibiting the azimuthal currents in a magnetic nozzle.

Thus from the study of detachment models the kinetic detachment model along with the resistive detachment seem the most feasible way to model the mechanism of detachment and will be examined.

CHAPTER IV

COMPUTATIONAL MODEL

Lattice Boltzmann method

The lattice Boltzmann method is used to find the Navier-Stokes and MHD equations from kinetic theory and Boltzmann's equations [9,10,11]. Once again the Boltzmann equation in its most basic form is shown below with the BGK collisional operator applied.

$$\frac{\partial f_\alpha}{\partial t} + \vec{c} \cdot \nabla f_\alpha = \frac{1}{\lambda}\left(f_\alpha - f_\alpha^{(eq)} \right) \tag{4.1}$$

This equation can be changed into the lattice Boltzmann equation shown below.

$$\frac{f_\alpha(x,t+\delta t) - f_\alpha(x,t)}{\delta t} + c\frac{f_\alpha(x+\delta x_\alpha, t+\delta t) - f_\alpha(x,t+\delta t)}{\delta t} = \frac{1}{\tau\varepsilon}\left(f_\alpha(x,t) - f_\alpha^{(eq)}(x,t) \right) \tag{4.2}$$

In this equation τ times ε has replaced λ where τ is the relaxation time and ε is the Knudsen number. A simplification can be made to this equation by assuming that c is the isothermal speed of sound at which the lattice particles propagate.

$$c = \frac{\delta x_\alpha}{\delta t} = \sqrt{3RT} \tag{4.3}$$

Additionally ε and dt can be set to be equal which leads the following form of the lattice Boltzmann equation.

$$f_\alpha(x+\delta x_\alpha, t+\delta t) - f_\alpha(x,t) = -\frac{1}{\tau}\left(f_\alpha(x,t) - f_\alpha^{(eq)}(x,t) \right) \tag{4.4}$$

The Boltzmann equation relates the probability density distribution functions to the collisions. The newly introduced τ_F is the fluid relaxation time which is related to the viscosity.

The goal of using the Boltzmann equation and kinetic theory is to find the Navier-Stokes and MHD equations. The Navier Stokes equations are shown below:

$$\frac{\partial \rho}{\partial t} + \nabla \cdot \left(\rho \vec{v} \right) = 0 \tag{4.5}$$

$$\frac{\partial \rho \vec{v}}{\partial t} + \vec{v} \nabla \cdot \rho \vec{v} = -\nabla p - \nabla \cdot \bar{\Pi} \tag{4.6}$$

To get these equations the LBE is expanded using a Taylor series expansion about dt, the Chapman-Enskog procedure, and an expansion of the time derivative [10,12]. As a result of these the following equations are produced in which e_{alpha} is the characteristic velocity vector.

$$\left[\frac{\partial}{\partial t_0} + \vec{e}_\alpha \cdot \nabla \right] f_\alpha^{\,0} = \frac{f_\alpha^{\,1}}{\tau_f} \tag{4.7}$$

$$\frac{\partial f_\alpha^{\,0}}{\partial t_0} + \left(1 - \frac{1}{2\tau_f} \right) \left[\frac{\partial}{\partial t_0} + e_\alpha \cdot \nabla \right] f_\alpha^{\,1} = -\frac{f_\alpha^{\,2}}{\tau_f} \tag{4.8}$$

The first and second moments of these equations give the following which must be related to the Navier Stokes equations.

$$\frac{\partial}{\partial t} \left(\sum_\alpha f_\alpha^{\,0} \right) + \nabla \cdot \left(\sum_\alpha e_\alpha f_\alpha^{\,0} \right) = 0 \tag{4.9}$$

$$\frac{\partial}{\partial t}\left(\sum_{\alpha} e_{\alpha} f_{\alpha}^{\,0}\right)+\nabla\cdot\left(\Pi^{0}+\delta t\left(1-\frac{1}{2\tau_{f}}\right)\Pi^{1}\right)=O\left(\delta t^{2}\right) \tag{4.10}$$

$$\Pi^{n}=\sum_{\alpha} e_{\alpha} e_{\alpha} f_{\alpha}^{\,n} \tag{4.11}$$

The proper equation must also be chosen for f_{alpha}^{eq} in order to model the shear stress terms, Π^0 and Π^1 correctly. The chosen equation is shown below so that the first and second moments correspond to the Navier-Stokes Equations.

$$f_{\alpha}^{(eq)}=\rho w_{a}\left[1+\frac{3}{c^{2}}\vec{e}_{\alpha}\cdot\vec{v}+\frac{9}{2c^{4}}(\vec{e}_{\alpha}\cdot\vec{v})^{2}-\frac{3}{2c^{2}}\vec{v}\cdot\vec{v}\right] \tag{4.12}$$

In this equation w_a is a weighting factor determined by the lattice structure. This particular equation has an incompressible limit and the Mach number must be .3 or less or the system will become unstable [9].

Viscosity can be calculated using the following equation [11].

$$\nu=\frac{\left(\tau_{f}-.5\right)}{3}c^{2}\delta t \tag{4.13}$$

The relationship between the relaxation time and viscosity are shown here. As the relaxation time increases, the viscosity increases and thus the macroscopic relationships are found from the intermolecular collisions.

Summing of these equations leads to density and momentum

$$\rho = \sum_{\alpha=1}^{N} f_\alpha \tag{4.14}$$

$$\rho v_\alpha = \sum_{\alpha=1}^{N} e_\alpha f_\alpha \tag{4.15}$$

The vectors in these equations have a specific direction determined by the lattice assembly of every molecule modeled using the LBM. The higher the amount of lattice structures, the greater the accuracy, producing a higher computational load. Specifically for the three dimensional flow the nineteen directional velocity structure, Q19D3 shown in Figure 12, is most often used and has had its accuracy and stability validated [6].

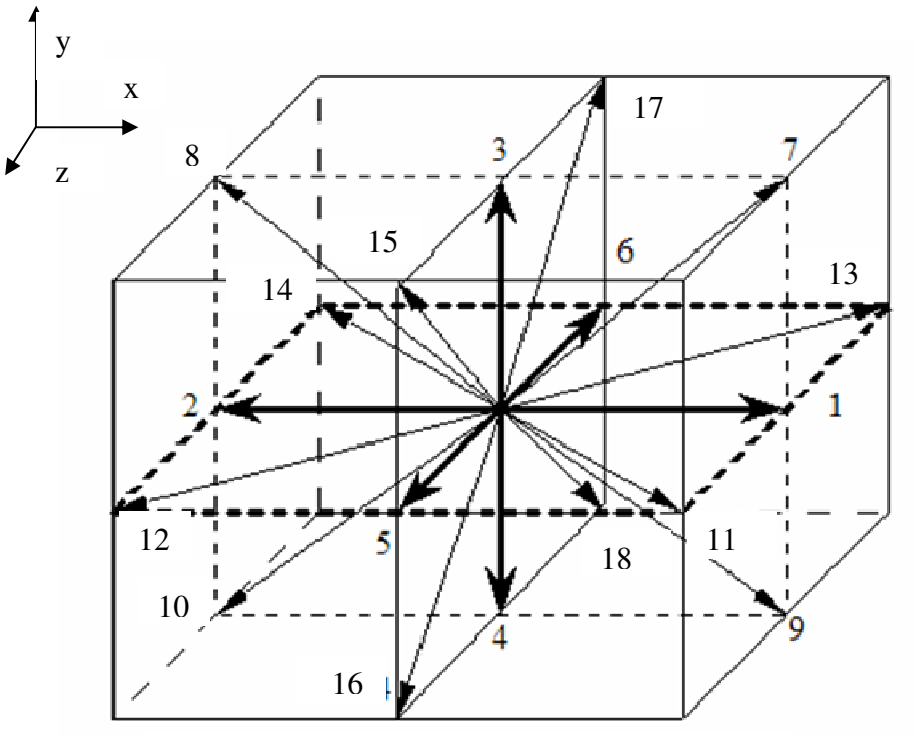

Figure 12. Q19D3 lattice [6]

The lattice Boltzmann method is a three phase process which begins with modeling the collisions, then propagates the information from the collisions through the lattice, and finally recovers the physical values.

The MHD version of the lattice Boltzmann method utilizes the Boltzmann equation used for kinetic plasma theory with the acceleration term replaced by the electromagnetic forces.

$$\frac{\partial f_\alpha}{\partial t} + \vec{c} \cdot \nabla f_\alpha + \vec{a} \cdot \nabla_c f_\alpha = -\frac{1}{\tau_f}\left(f_\alpha - f_\alpha^{(eq)} \right) \tag{4.16}$$

The Boltzmann equation can be used to model the ions or electrons separately in a two fluid model, or model them together as a single fluid in a one fluid model. The one fluid model is used to obtain the MHD equations found in the previous MHD section. Modeling the MHD equations requires calculations of density and momentum much like the regular lattice Boltzmann. However the magnetic induction equation must also be modeled and for this an additional function **g** is used [12].

Two forms of the lattice Boltzmann equation can be used to develop the momentum equation for the MHD-LBM. The first of these is the body force formulation which calculates an external acceleration term to be used in the Boltzmann equation. The extended equilibrium formulation (EEF) neglects the acceleration term and instead extends the equilibrium formulation by adding Maxwell's stress tensor. The EEF method has been verified and proven to be accurate and stable and will be used [12].

The EEF changes only the equilibrium function and describes the Lorentz force as a Maxwell's stress divergence term.

$$\frac{\partial}{\partial t}\left(\rho\vec{v}\right)+\nabla\cdot\left(p\vec{v}\vec{v}+p\bar{\bar{I}}+\frac{1}{2\mu_0}B^2\bar{\bar{I}}+\frac{1}{\mu_0}\vec{B}\vec{B}\right)+\nabla\cdot\left(\rho\upsilon\bar{\bar{S}}\right) \tag{4.17}$$

The EEF method is chosen primarily due to its ease of implementation while also being the most developed.

The magnetic induction equation is calculated by a similar lattice Boltzmann formulation.

$$\frac{\partial g_{\beta j}}{\partial t}+\Xi\cdot\nabla g_{\beta j}=-\frac{1}{\tau_g}\left(g_{\beta j}-g_{\beta j}{}^{(eq)}\right) \tag{4.18}$$

Although the magnetic field is not physically described by kinetic theory as implied by this equation, the lattice Boltzmann equation can model the magnetic induction equation because it is a conservative hyperbolic equation like the momentum equation and can be numerically modeled in a similar method.

The discretized form of this equation is then expanded in the same way as the original LBM method. There is an important difference however between how the equilibrium function models the magnetic induction and the momentum. The difference arises from the presence of symmetric divergence terms in the momentum equation and anti-

symmetric terms in the magnetic divergence equation. This issue is resolved by using the following equation for the equilibrium function for the magnetic induction [12].

$$g_{\beta j}^{(eq)} = w_\beta \left[B_j + \frac{4}{c}\left(v_i B_j - B_i v_j \right) \right] \tag{4.19}$$

The magnetic diffusivity is related to the relaxation parameter through the following equation.

$$\sigma = \frac{\left(\tau_g - .5 \right)}{4} c^2 \delta t \tag{4.20}$$

The lattice structure used for the magnetic field is different from the structure used for the velocity field. The reason for this lies in that the magnetic field is described by vector distribution function and the velocity field by scalar distribution functions. Because the magnetic field uses the vector distribution functions it can require a smaller lattice structure of Q7D3, seen in Figure 13, which has been validated for accuracy [12].

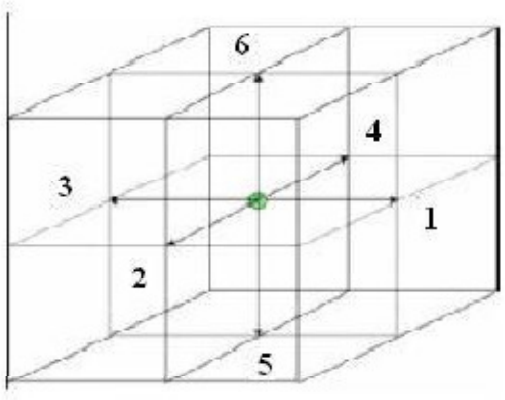

Figure 13. Q7D3 lattice [6]

The previous formulations for LBM used the single relaxation time parameter, with only single parameters for τ_f or τ_g. This works well for low Reynolds number and simple geometry flows but fails otherwise. A multiple relaxation time method is needed to solve these cases while improving accuracy and enhancing stability. This method redefines the probability distribution functions with different moments and a specific relaxation parameter to each. A large transformation matrix M is used to compute these moments through linear mapping with another matrix S known as the diagonal relaxation matrix composed of the different relaxation times.

The MRT method is then adapted for MHD-LBM with the EEF by separating into separate velocity and magnetic field parts. The velocity fields are modeled with the MRT method while the magnetic field is modeled with the SRT method as no method has yet been found to model the magnetic field with MRT. Differences between the MRT and SRT formulation start to occur at higher Reynolds numbers, while they generally agree at lower Reynolds numbers [6]. MRT remains stable at much higher value Reynolds numbers.

Computational model

The code used to model the behavior of the plasma is a C++ code that makes use of the lattice-Boltzmann method to solve the linearized Boltzmann equation and then the MHD equations. The lattice-Boltzmann method integrates the linearized Boltzmann equation along characteristic velocities chosen to satisfy a specific symmetry on the lattice and

then finds macroscopic physical properties such as density and velocity. Both single-relaxation-time and multiple-relaxation-time LBMs are useable.

The computational domain is rectangular with a variable mesh size. Among the mesh sizes used in this research are 64x32x32 and 128x64x64. The domain has x, y, and z directions with the x direction defined as the axial direction which is the larger of the three axis. The cases were run for differing time steps based on the mesh size which ranged from 700 to 2000 steps. These values were chosen by a convergence study which sought to establish a point at which the flow through the nozzle reaches a steady state.

Plasma enters the domain, seen in Figure 14, through an inlet on an x-plane at the beginning of the domain. The portion of this face that is not the inlet has no slip, bounce-back for wall, and insulating boundary conditions applied to it, while the inlet has conducting and bounce-back for uniform flow boundary conditions applied to it. Periodic boundary conditions are applied at non-axial boundaries while extrapolations boundary conditions are applied at the downstream wall. At the beginning of the simulation the velocity is zero everywhere except for at the inlet.

The magnetic fields in the domain are created by circular current loops lying in the x-plane. The magnetic fields produced by these loops are found through elliptic integrals based on the Biot-Savart law [26].

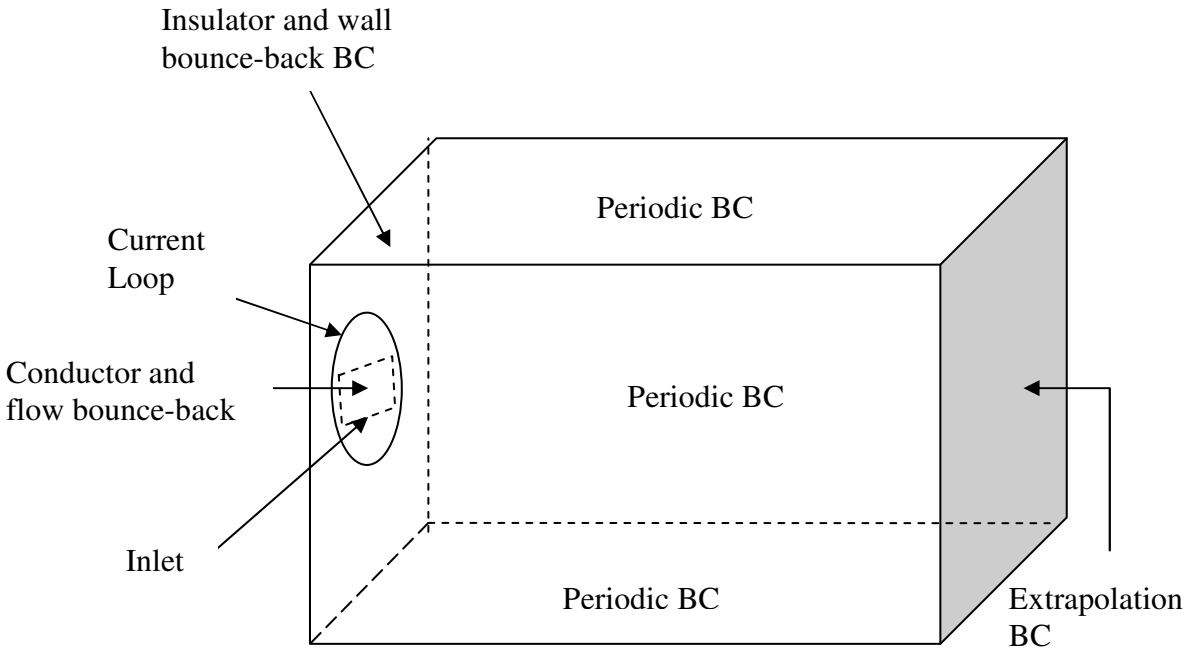

Figure 14. Computational domain and boundary conditions

Modifications were made to this code created at Texas A&M University that was used for turbulence studies in rectangular jets among other topics [5,6,7,8]. This older version of the code only supported two current loops which have the same size and current with any changes in this having to be hard coded. The current code allows for multiple loops, individual loop sizes, individual loop currents, and additional new, variable parameters that are specified in an input file instead of having to be hardcoded.

Singularities in the computations by the code were addressed and corrected as well. Particularly the growth of the magnitude of the magnetic field near the current loops was

examine and corrected. Other singularities have also been quantified and verified due to the limitations of the code as being incompressible and limited to low Mach numbers.

CHAPTER V

RESULTS

Parametric study

The goal of the parametric study was to examine the behavior of the plasma flow under variations of certain input parameters. The domain, seen in Figure 15, is rectangular in shape with an inlet for the plasma and a current loop inside of the domain to produce a magnetic field. The grid size chosen was 64x32x32 for the parametric study.

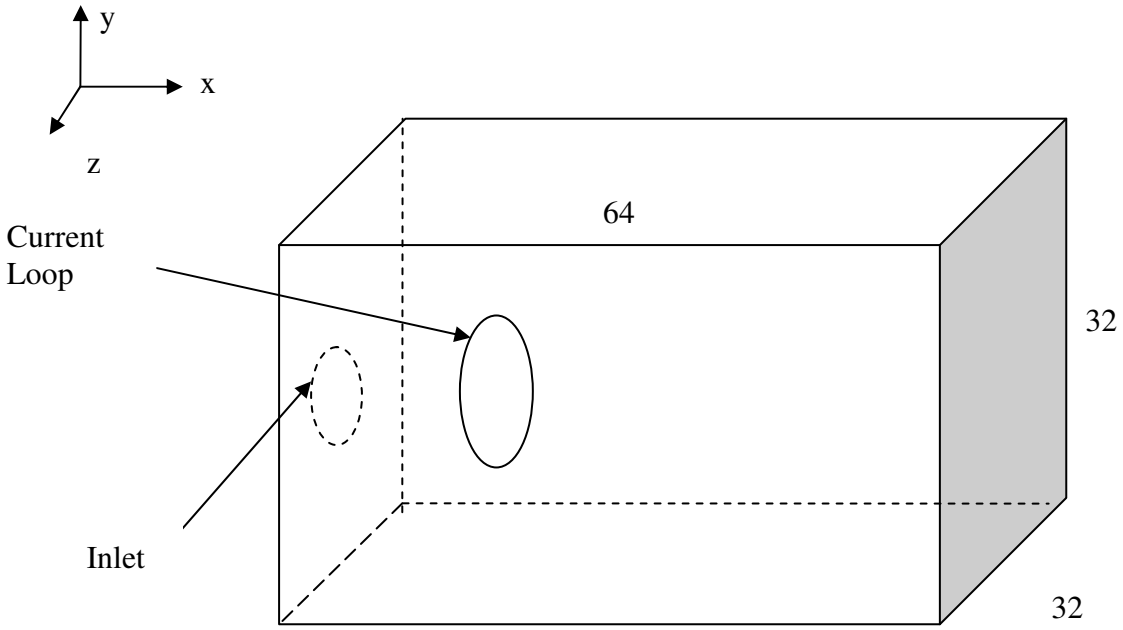

Figure 15. Parametric study computational domain

The first step in the parametric study was to establish a base case to compare with other cases. This base case was found by choosing a flow that did not exhibit extreme

behavior so that variations in the flow can be seen as the parameters that characterize the flow are varied. Increasing time steps were run until convergence to a steady state was established. In the figures of the following sections the base case is always shown as the middle velocity flow field domain. In these figures the contour shows the magnitude of the velocity in the x-direction while the stream traces show the flow velocity vectors. The magnetic field for all of the cases is shown below in Figure 16 with the contour showing the magnitude of the magnetic field and the stream traces showing the magnetic field lines.

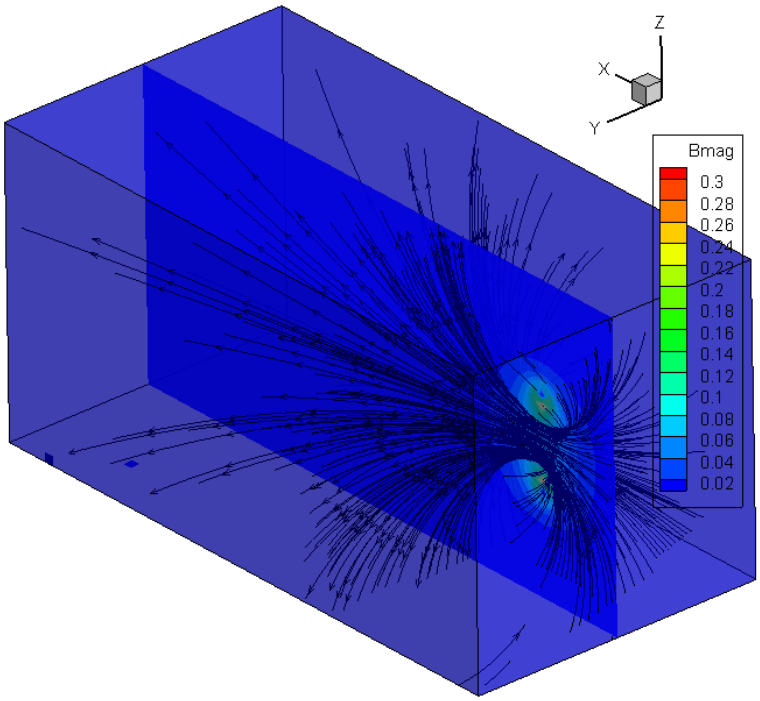

Figure 16. Magnetic field stream traces and contours for parametric study

In the parametric study the velocities and input parameters can only be compared qualitatively to the expected real world values and not quantitatively as all values are scaled and non-dimensionalized. The behavior of the plasma flow as a result of parameter variation was found by changing the value of a single input parameter while keeping the others constant. The limits of the input parameters were found in a similar fashion, but with additional cases ran to study the effects on the limits of one parameter when other parameters are varied. The limitations for the values of the parameters was found to be the velocity due to the low Mach number assumptions, limiting the code to running cases in which the velocity in the domain is less than .3 times the speed of sound.

Inlet velocity

The first parameter examined was the inlet velocity. The ranges of the Reynolds number and the magnetic Reynolds number examined were from .03 to 9 and .04 to 12 respectively with increasing velocity increasing both Reynolds numbers. As the inlet velocity was increased, as seen in the right domain of Figure 17 there was less flow around the current loop and detachment of the flow from the applied magnetic field lines. Conversely as inlet velocity is decreased, as seen in the left domain of Figure 17, there is more flow around the current loop and more attachment to the magnetic field lines. This behavior of greater detachment with greater velocity agrees with both theory and experimental results. Thus for the purpose of plasma propulsion utilizing magnetic nozzles, high axial velocities will produce greater detachment and are desirable. The

limitation of the model is reached when the flow velocities approached the low Mach number limit.

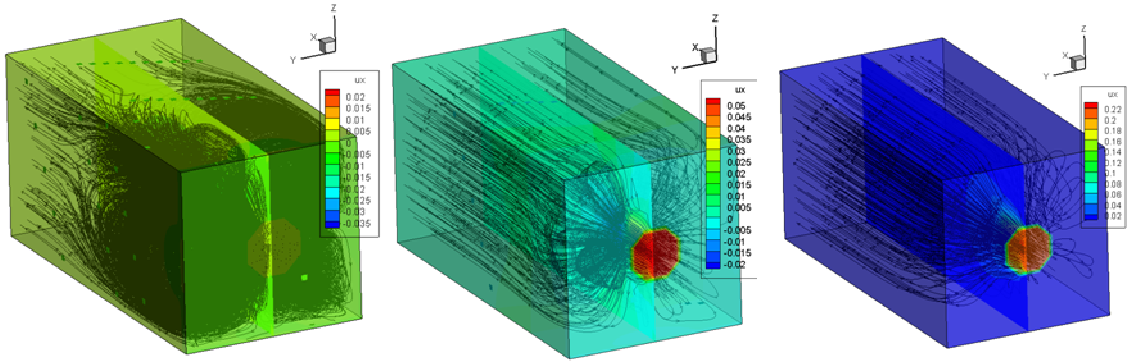

v_{inlet} = .001 v_{inlet} =. 05 v_{inlet} = .2

Figure 17. Inlet velocity variation

Pressure gradient

The next parameter investigated was the pressure gradient. The variation of the pressure gradient did not affect either Reynolds number so a constant Reynolds number of 1.5 and a constant magnetic Reynolds number of 2 were used. As the pressure gradient was increased to larger positive values the flow was accelerated by a favorable pressure gradient as seen in the right domain of Figure 18. Conversely as the pressure gradient was decreased to more negative values the flow was decelerated and even reversed by an adverse pressure gradient as seen in the left domain of Figure 18. The sign of the pressure gradient term may be contrary to normal notation but is defined in this manner

for the code. Thus higher positive pressure gradients produce higher velocities and lead to greater detachment and vice versa for negative pressure gradients. From this behavior it can be inferred that favorable pressure gradients produce greater detachment and are desirable in plasma propulsion devices with magnetic nozzles. The limits of the model are reached when the pressure gradient is too high in either direction causing velocities greater than the low Mach number limit of LBM.

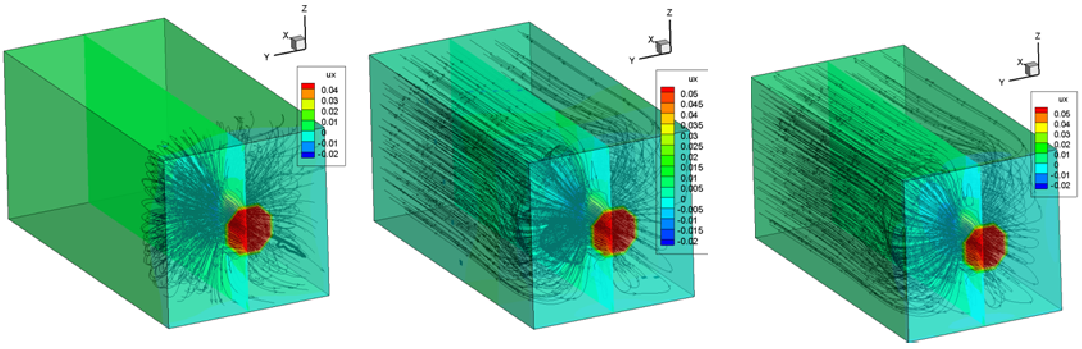

dpdx = -.0001 dpdx = 0 dpdx = .00001

Figure 18. Pressure gradient variation

Loop current

The variation of the current in the loop also had a distinct effect on the flow of the plasma. The variation of the loop current did not affect either Reynolds number so a constant Reynolds number of 1.5 and a constant magnetic Reynolds number of 2 were used. As the current was increased, as seen in the right domain of Figure 19, the strength

of the magnetic field was increased. This causes more flow to be attached to the applied magnetic field lines and causes flow around the current loop. When the current was decreased, as seen in the left domain of Figure 19, the strength of the magnetic field was decreased causing more detachment from the applied magnetic field lines. This behavior agrees with both theory and physical results. Thus in systems employing magnetic nozzles the current used has to be very carefully chosen as it can prevent detachment but still has to have the necessary strength to contain the flow and convert thermal or gyro energy to axial velocity. The maximum current able to be used was limited because when high values of current are used strong magnetic fields are created which caused the flow to be compressed significantly inside the current loop. This compression accelerates the flow to velocities beyond the low Mach number limit similar to physical nozzles.

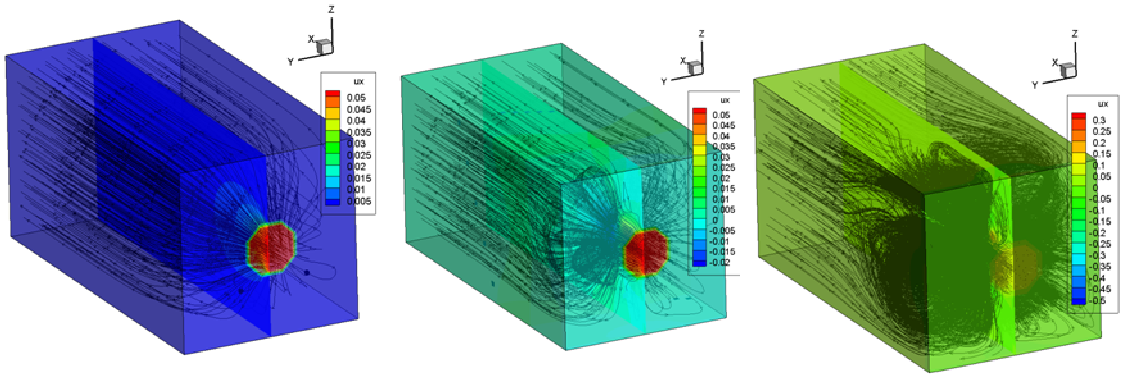

I = 100 I =1000 I = 3500

Figure 19. Loop current variation

Loop radius

Variation of the current loop radius also had a distinct effect on the flow in the domain. The variation of the loop radius did not affect either Reynolds number so a constant Reynolds number of 1.5 and a constant magnetic Reynolds number of 2 were used. As the radius was decreased, as seen in the left domain of Figure 20, the magnetic field inside the loop was increased. Conversely as the radius was increased, as seen in the right domain of Figure 20, the magnetic field inside the loop was decreased. These increases and decreases in magnetic field strength increase and decrease attachment to the applied magnetic field respectively. This may not readily be seen in Figure 20 because some of the plasma does not flow though the smaller radius because the inlet becomes larger than the current loop. The behavior experienced by varying the loop radius agrees with theory and physical results.

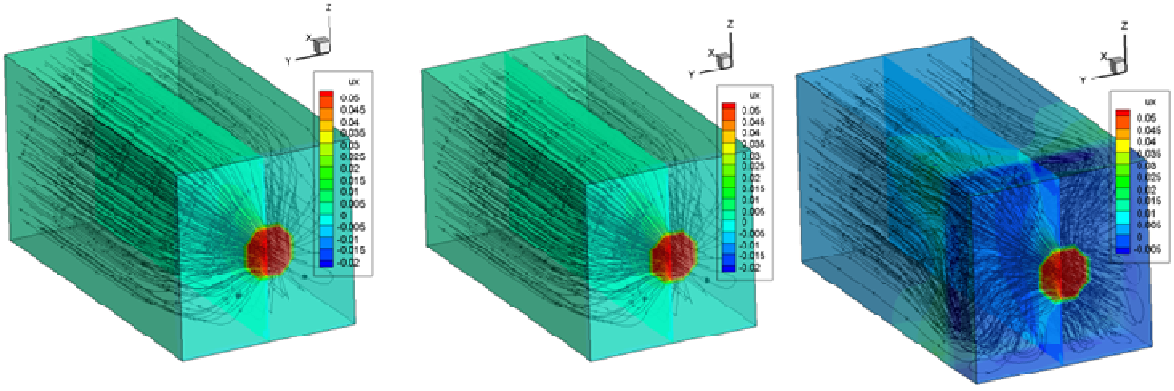

R = 1 R =5 R = 15

Figure 20. Loop radius variation

Magnetic relaxation time

The magnetic relaxation time had distinct effects on the behavior of the plasma. The Reynolds number and the ranges of the magnetic Reynolds number were a constant 1.5 and .001 to 1000000 respectively with increasing magnetic relaxation time increasing magnetic Reynolds number. As the relaxation time was increased the diffusive behavior was increased. This is also seen in the magnetic Reynolds number decreasing with increasing relaxation time. Increasing this diffusive behavior caused the effects of the magnetic field to be diffused by the plasma. This diffusion essentially decreased the effect that the magnetic field had on the flow. As seen in Figure 21 as the magnetic relaxation time was increased, the effects of the magnetic field on the flow were decreased and the detachment increased. Thus from this behavior, for detachment

purposes plasmas with high magnetic relaxation times are desirable, however this can also affect the positive effects that the magnetic field have, such as converting thermal and gyro energy to axial energy. The high magnetic relaxation times seem to produce resistive detachment as predicted by theory. The limits of the relaxation time were caused by Equation 6.20 and also by creating strong magnetic field effects inside the current loop that accelerate the flow. The effects of the magnetic relaxation time on the flow agree with both theory and physical behavior.

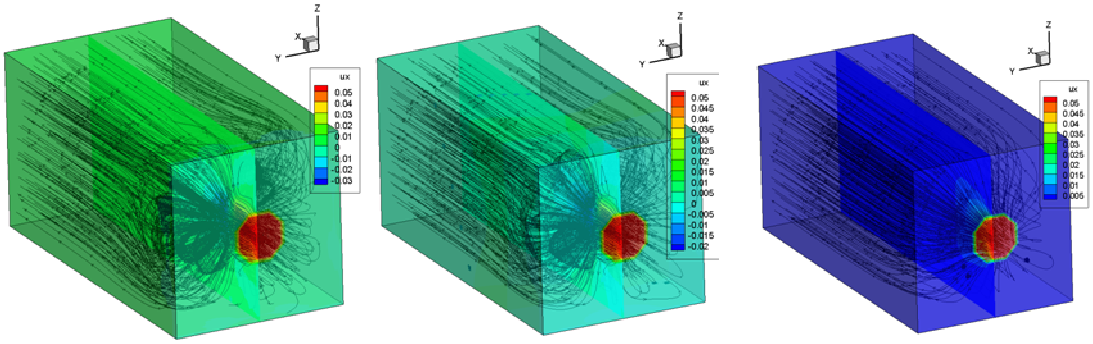

τ_B = .500001 τ_B =1.0 τ_B = 100

Figure 21. Magnetic relaxation time variation

Fluid relaxation time

The plasma flow was affected by the fluid relaxation time in specific ways. The ranges of the Reynolds number and the magnetic Reynolds number were from .01 to 75 and a constant 2 respectively with increasing fluid relaxation time increasing Reynolds number. As the fluid relaxation time was decreased, the viscosity of the fluid was decreased. This decrease in the viscosity increased the Reynolds number. As seen in Figure 22 below, as the fluid relaxation time was decreased the flow around the current loop increased, while increasing the relaxation time decreased the flow around the current loop. High relaxation times cause high viscosities which cause the effects of the magnetic field to diffuse quickly. Thus higher fluid relaxation times cause less flow around the current loop and more detachment. Similar to the magnetic relaxation time, high fluid relaxation times can then be inferred to be good for the purpose of detachment, however once again the other affects of the magnetic field such as converting thermal and gyro energy to axial energy are also affected. Again the high relaxation time seems to produce resistive detachment of the plasma. These results agree with those predicted by both theory and experimental results.

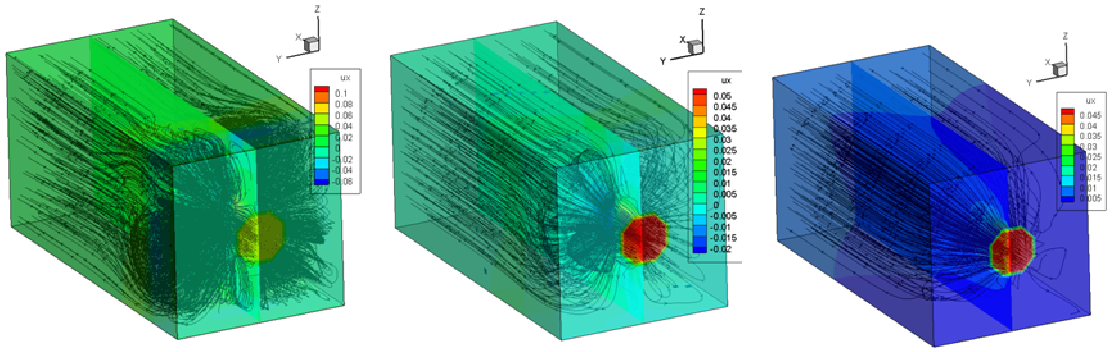

$\tau_F = .55$ $\tau_F = 1.0$ $\tau_F = 50$

Figure 22. Fluid relaxation time variation

Magnetic nozzle study

The goal of the magnetic nozzle study was to simulate real world systems, match results of other computational models, and examine detachment mechanics. The real world system selected was the Variable Specific Impulse Magnetoplasma Rocket (VASIMR). VASIMR is a magnetoplasma propulsion device composed of ionization, cyclotron heating, and magnetic nozzle sections as seen in Figure 23 [2].

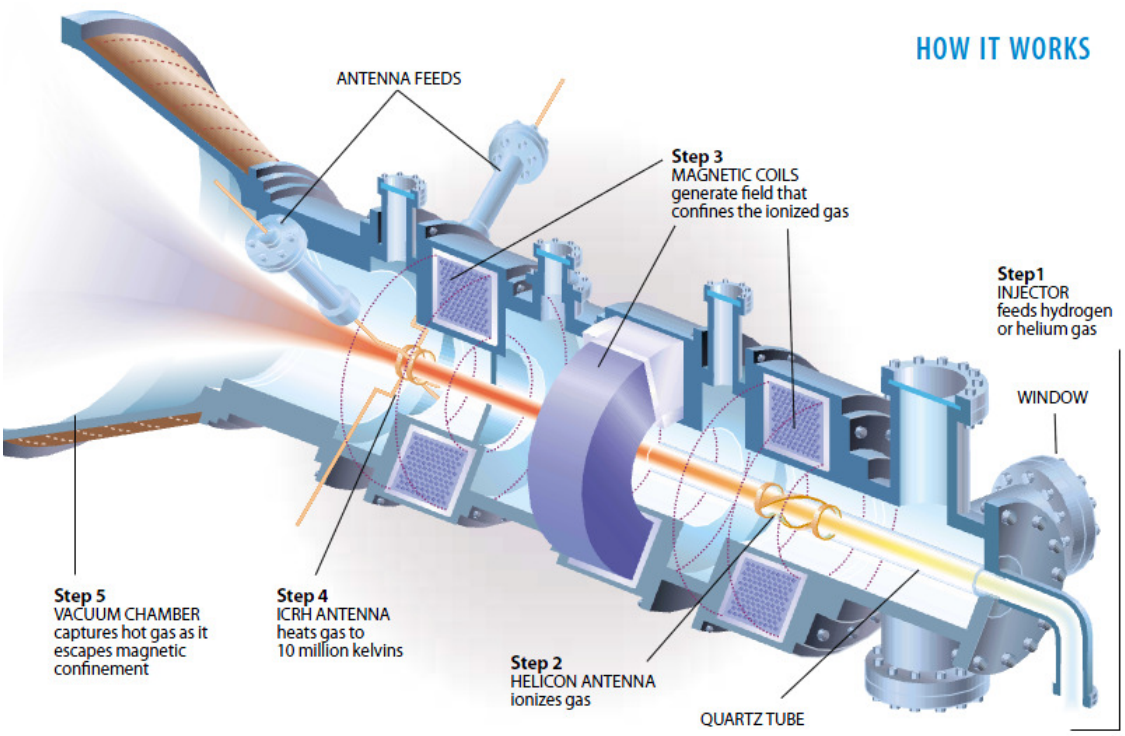

Figure 23. VASIMR schematic [2]

The primary region of interest is the magnetic nozzle which comprises the computational domain of this study. To simulate the magnetic nozzle the conditions before the magnetic nozzle are required to be known so that they can be used as initial conditions for the plasma and boundary conditions for the calculations in the magnetic nozzle. Due to the non-dimensional and scaled values inherent in the LBM model used, non-dimensional quantities such as the Reynolds number and magnetic Reynolds numbers were used as these inputs. In Table 1 below a range of values for both Reynolds numbers in VASIMR engines are shown. These values were obtained from literature and from calculations done by J.V. Shebalin [3,5,14,27].

Table 1. Range of Reynolds numbers in VASIMR

Magnetic Reynolds Number	Reynolds Number
5-150	.001-.1

The specific Reynolds Numbers chosen and the parameters resulting in these Reynolds numbers are shown below in Table 2. Note however that the temperatures and densities serve only as reference and were not the actual input quantities, only non-dimensional quantities were used.

Table 2. Reynolds numbers used in simulation

Te	Ti	Magnetic Reynolds Number	Reynolds Number	n_p
5 eV	10 eV	8.125390596	0.046983741	1E+18

The chosen parameters correspond to a power level of 395 kW or 24 kW VASIMR Thruster and are comparable with other computational model studies [3,19].

Demonstrating detachment from the magnetic field lines in a way similar to physical results and results by other computational methods is the primary component of the comparison to VASIMR that is examined. One mechanism for this detachment is caused by the kinetic energy of the plasma exceeding the magnetic energy. This ratio is shown by the previously mentioned parameters β and Alfvén Mach number which when

greater than one indicates a higher kinetic energy than magnetic energy. When the flow reaches a β of unity or higher it will detach from the magnetic field [18]. Additionally resistive detachment by the plasma will also be examined as a mechanism for detachment.

When modeling cases similar to VASIMR a mesh size of 128x64x64 was used and time steps were run until a steady state was achieved. Due to having no non-dimensional parameters associated with the magnetic field, other than β and Alfvén Mach number, a parametric study of loop currents had to be conducted until correct and comparable results were found. Figure 24 shows a schematic of the domain used to simulate VASIMR. The characteristics of this domain were chosen to both simulate VASIMR and produce domains similar to those used by other computational models [14,

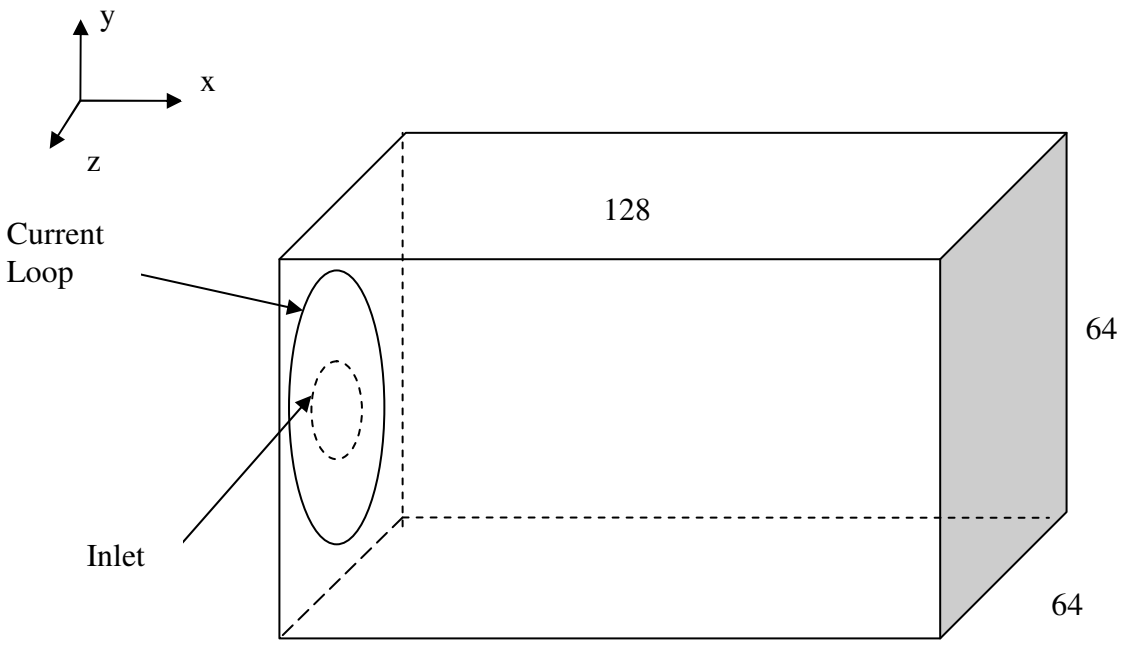

Figure 24. VASIMR computational domain

Figure 25 shows a successful case which demonstrated plasma detachment. In this figure the top domain shows the magnetic field lines with a contour of the Alfvén Mach while the bottom domain shows the velocity field lines with a contour of the Alfvén Mach.

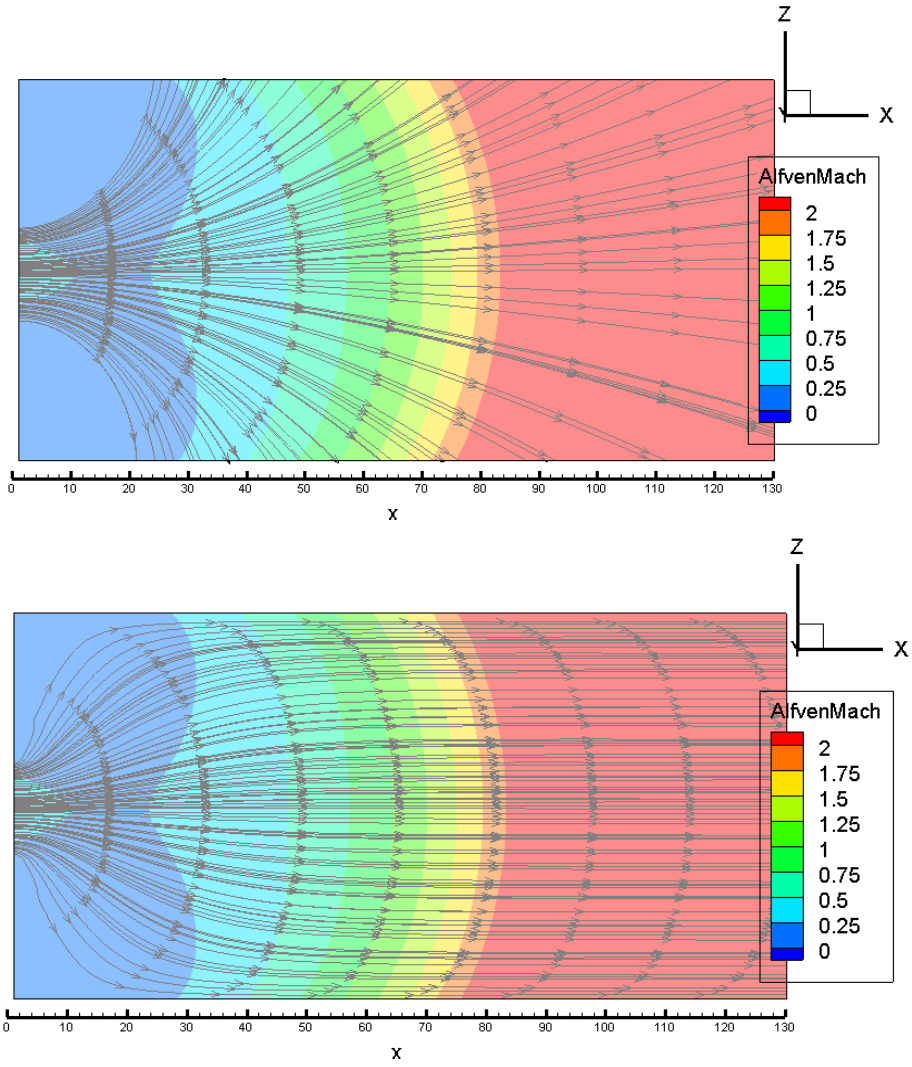

Figure 25. Top: Magnetic field lines on Alfvén Mach contour, Bottom: Velocity field lines on Alfvén Mach contour

In Figure 25 it is seen that the velocity field lines do not flow in the same direction as the magnetic field lines demonstrating detachment. The Alfvén Mach contours also show that this separation seems to result from increasing Alfvén Mach number, agreeing with theory. However, due to the detachment violating the "frozen-in" condition and separating from the magnetic field lines, the detachment mechanism seems to be a combination of kinetic and resistive detachment. In Figure 26 an inset of Figure 25 is shown in comparison to similar results found by another computational model.[22] The domains between the two models are slightly different with the model from literature using a solenoid instead of single loop to produce the magnetic field while also containing the plasma inside the solenoid for a portion of the domain. This difference does not greatly affect the behavior of the plasma after it leaves the solenoid, which is the region of interest. The similar behavior between the two models showing the detachment of the plasma at Alfvénic Mach numbers above unity is visible and confirms that both models are producing similar behavior.

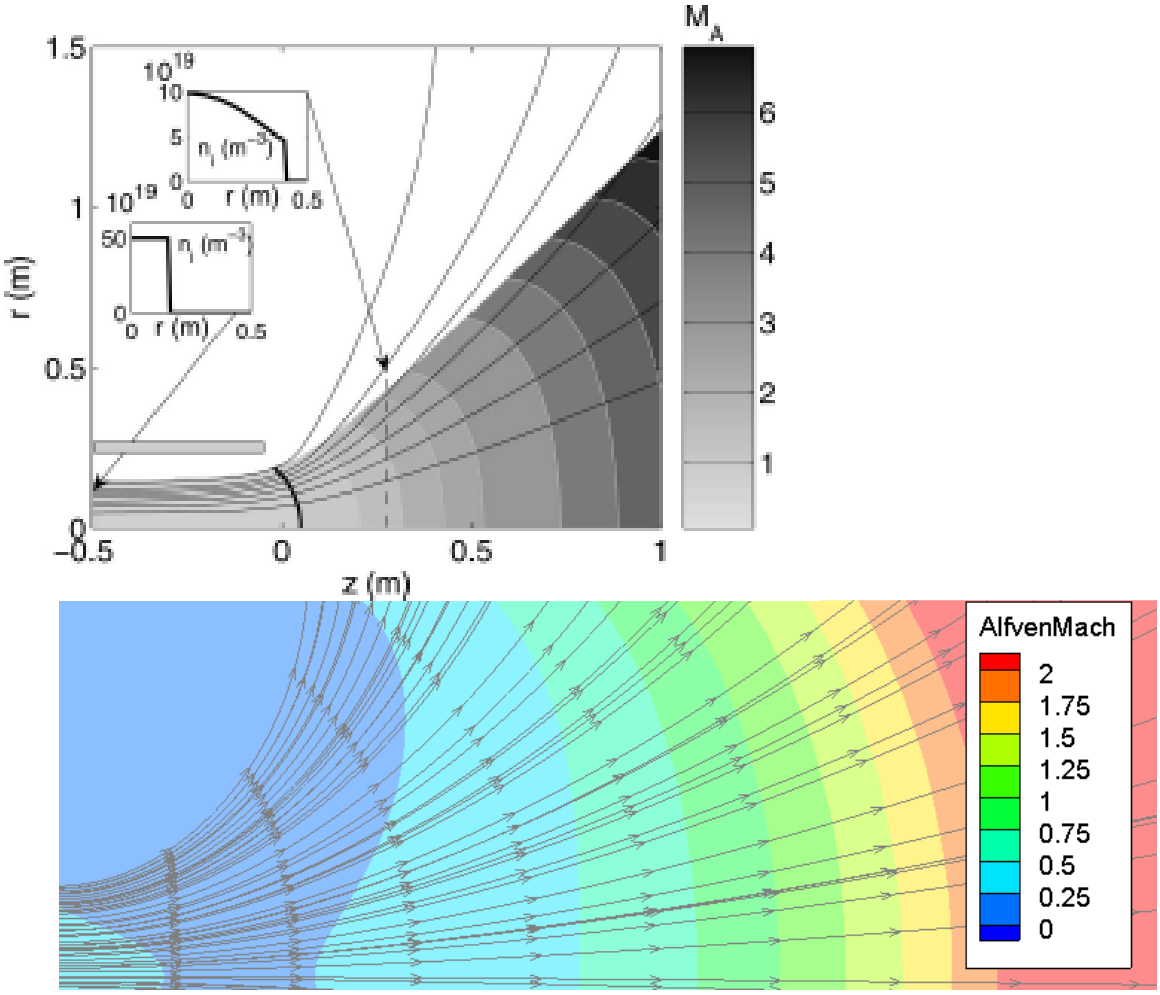

Figure 26. Top: Alfvén Mach contour from literature [22], Bottom: Inset from Figure 24 with magnetic field lines on Alfvén Mach contour

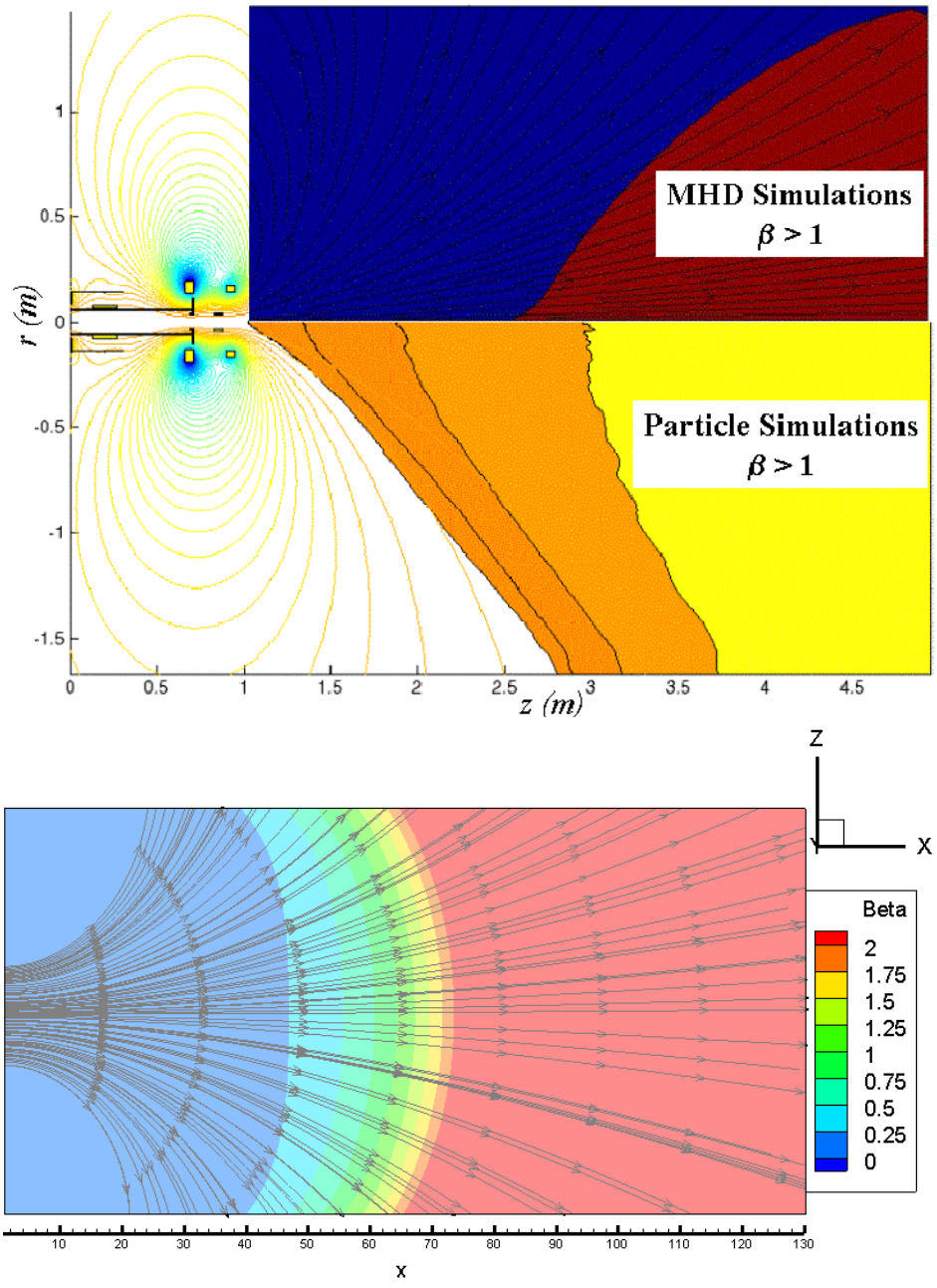

Figure 27. Top: Magnetic field lines with β contour from literature [16], Bottom: Magnetic field lines and β contour from test case.

A comparison using the parameter β with another computational model is also shown in Figure 27. Once again detachment is shown by both methods, while the detachment mechanism also behaves similarly by showing detachment at super-Alfvénic Machs.

Comparing the axial and perpendicular kinetic energies also produced interesting results. From Figure 28 the effects of the magnetic field on the flow are seen as it converts some of the initially purely axial flow at the inlet to perpendicular flow. This also shows that as the flow expands into the domain it loses velocity, which is expected for low, incompressible Mach numbers ran. Figure 29 shows the ratio of the axial kinetic energy to the perpendicular kinetic energy and shows that as the flow moves away from the strong magnetic field, the ratio increases. This increase in the ratio shows that the flow gains axial kinetic energy compared to perpendicular kinetic energy. This creates both the detachment of the plasma and demonstrates the conversion of some gyro energy to axial energy, even though initially some axial energy is converted to gyro energy.

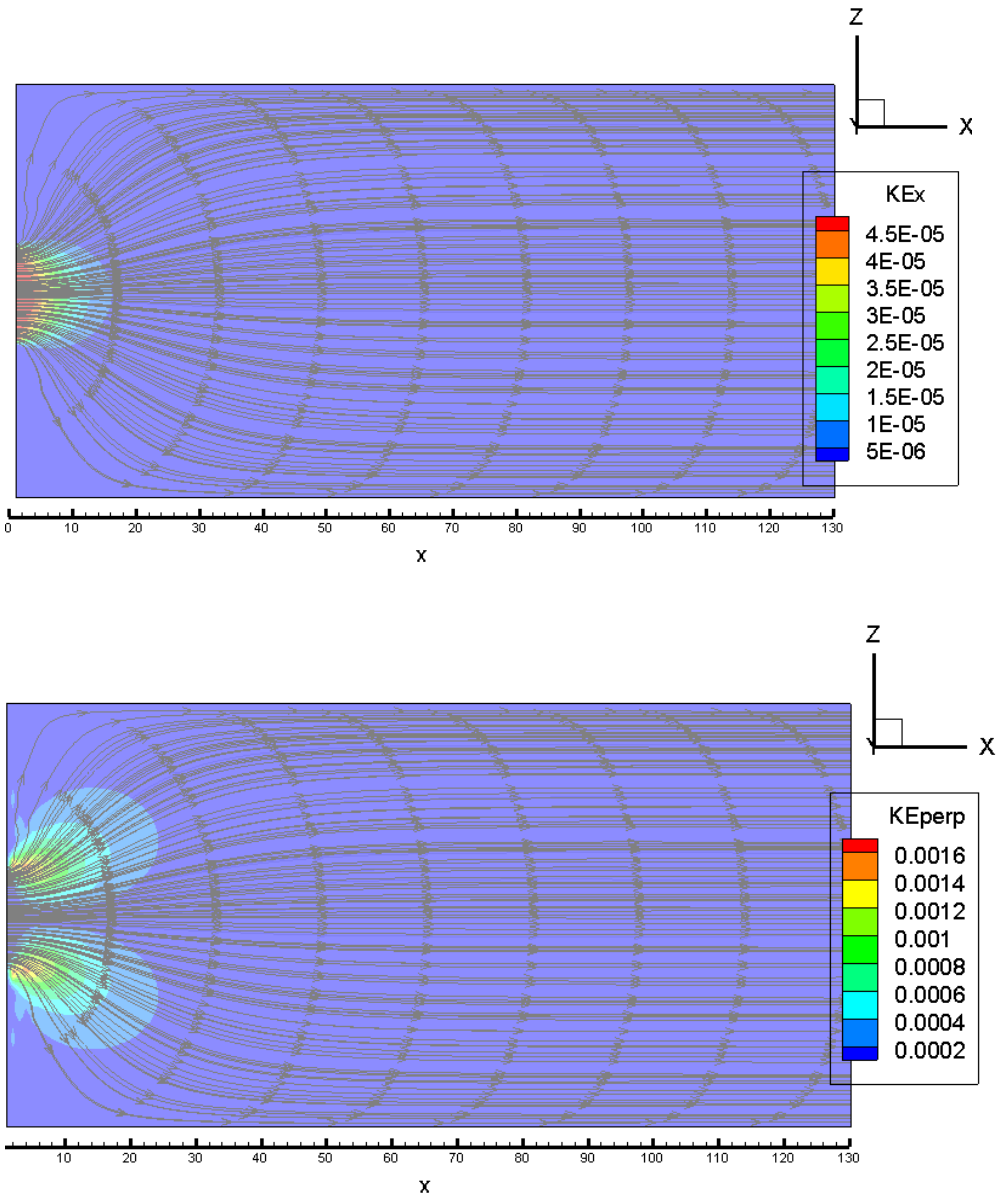

Figure 28. Top: Axial kinetic energy, Bottom: Perpendicular kinetic energy.

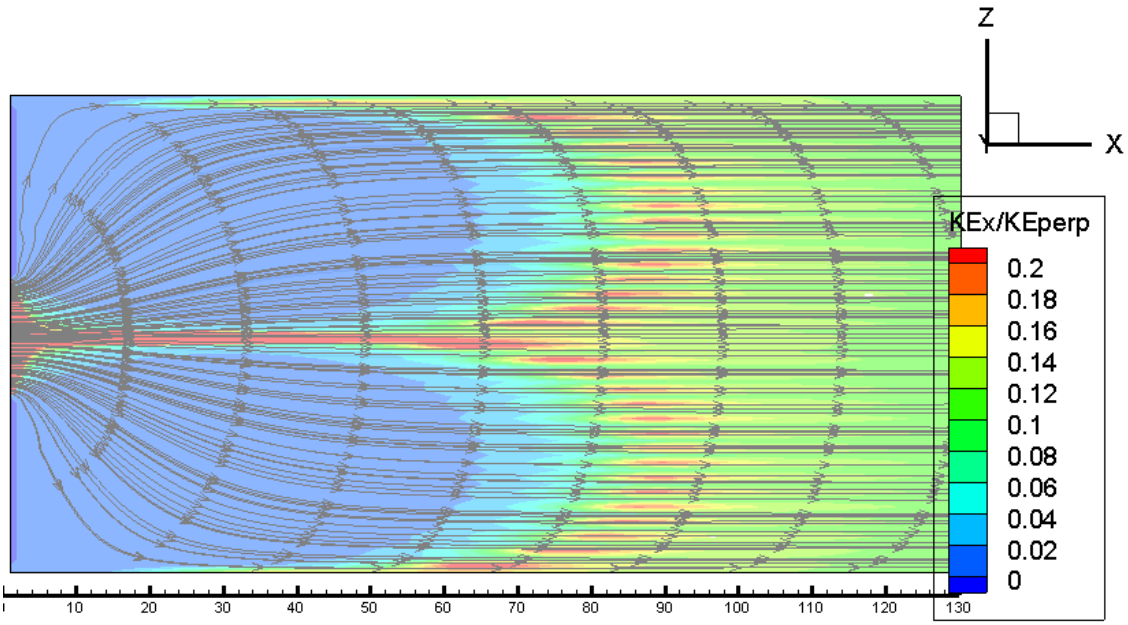

Figure 29. Ratio of axial kinetic energy to perpendicular kinetic energy.

A final case is shown with the chosen Reynolds numbers to demonstrate when detachment is not present. This case is shown in Figure 30 with an Alfvén Mach contour and velocity streamlines. The velocity steam lines are clearly shown bending back to the conducting wall as they are attached to the magnetic field lines. The conducting wall has a no slip condition applied to it and forces the flow along it which eventually causes it to bend back, but the reverse flow is clearly shown. The Alfvén Mach numbers are also shown to be much less and only approach unity far away from the inlet.

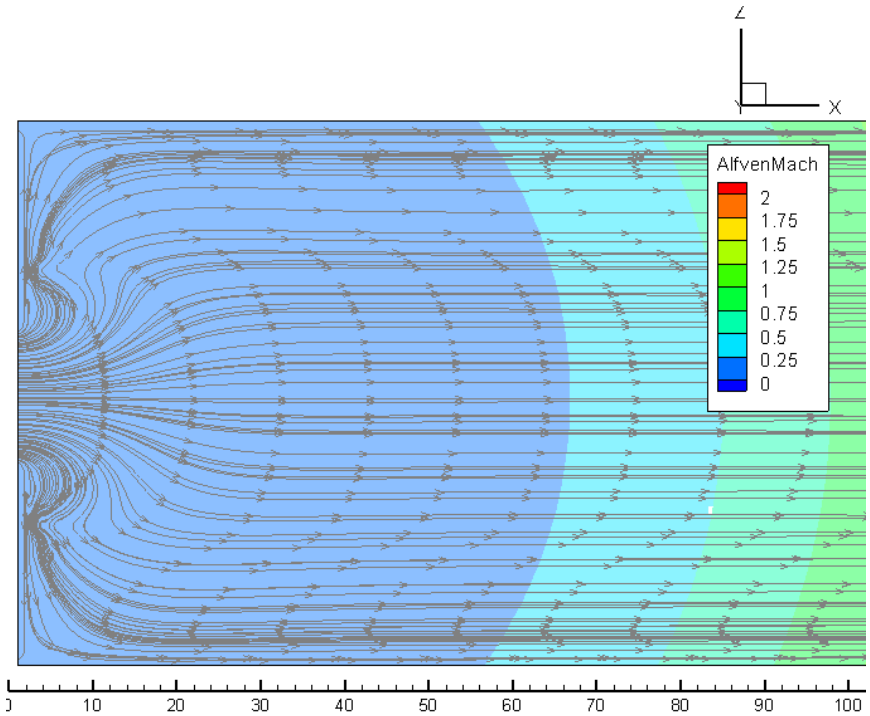

Figure 30. Plasma flow with high magnetic field and little detachment

Convergence was also examined to determine the best domain size and the amount of iterations for which the test cases were ran. Figure 31 shows the convergence values for different domain sizes ran for 1000 time steps. As the domain size increased the convergence increased as seen in the L2 Norms decreasing. Beyond the domain size of 128x64x64 it is seen that the next higher domain size only increased convergence marginally. The convergence seems to approach an asymptote. This asymptote can be more closely approached, but this requires larger domains which lead to longer run times with only marginally better convergence, which is impractical. Thus 128x64x64 was chosen for its relative accuracy and reasonable runtime. As the cases were ran for more iterations the cyclical pattern continued while damping to a specific value as seen.

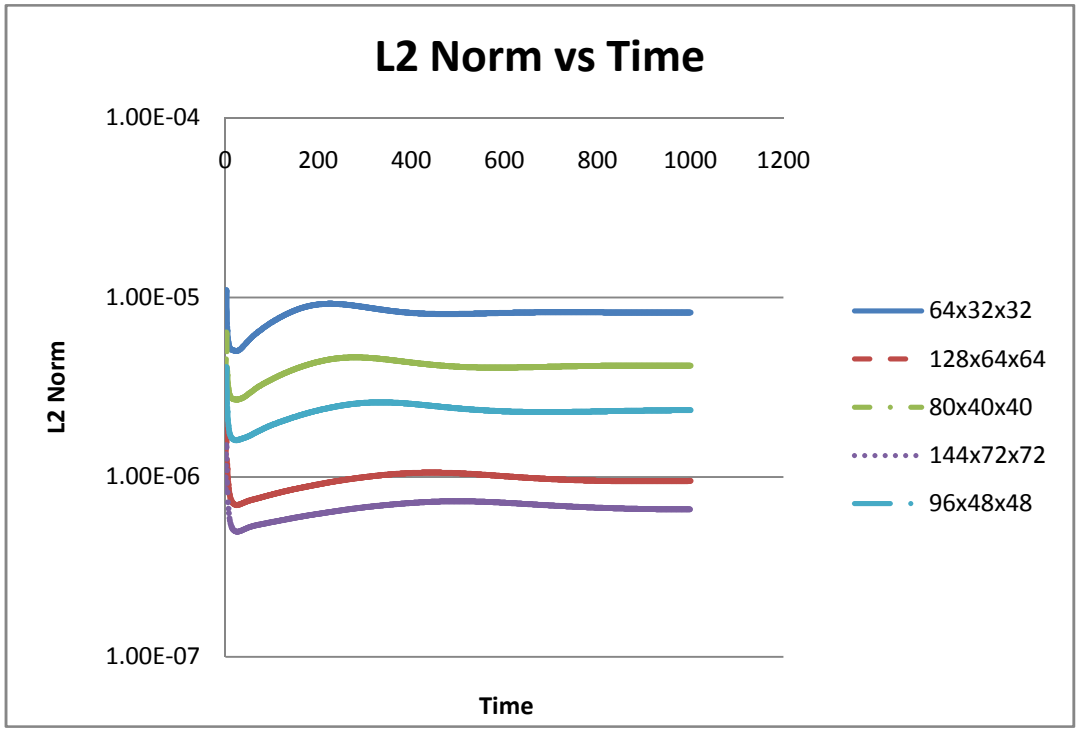

Figure 31. L2 Norms versus time for varying domain sizes

Convergence was additionally examined by comparing the axial velocity along the center line of the domain between different domain sizes and time steps as seen in Figure 32. The short time step shown was run for 1000 iterations while the long time step was run for 2000 iterations. From this figure it is seen that as the domain size is increased the centerline axial velocity seems to converge to a specific curve. The domain size 128x64x64 was chosen once again because it was seemed to be close to the convergence point while also maintaining reasonable run times and producing good results. The longer time case ran also shows a slightly different axial velocity graph, the small change in results however does not merit doubling the run time of the model.

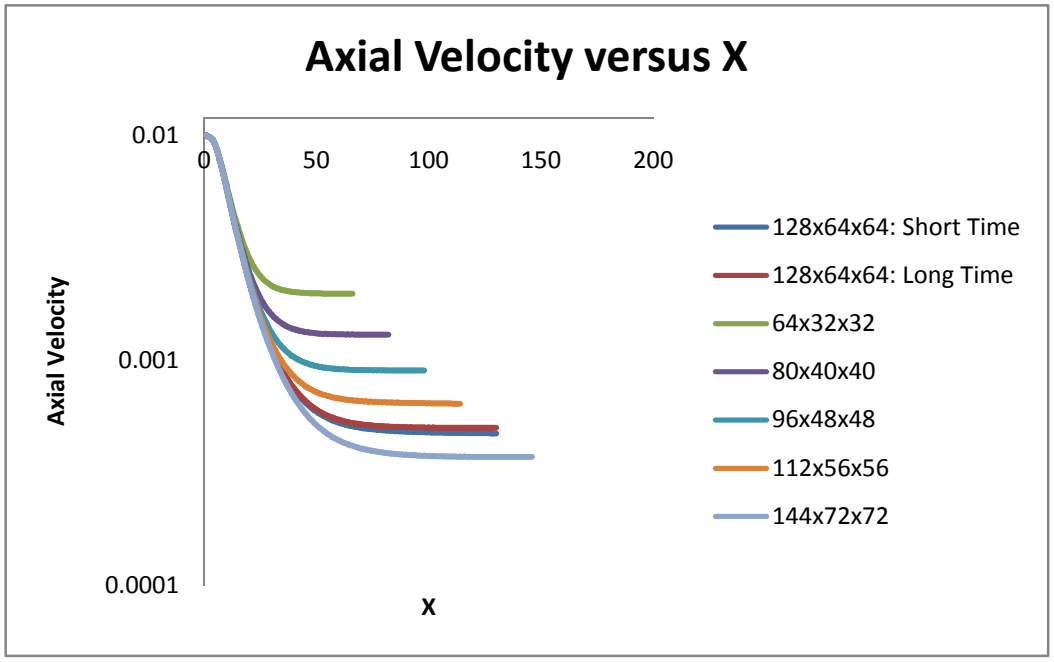

Figure 32. Axial velocity versus axial position for varying domain sizes and time-steps

The machine used to run these cases had two Gigabytes of RAM with a 2.16 GHz Centrino Duo Processor. A domain size of 128x64x64 ran for 1000 time-steps took approximately 5 hours to run, while a domain size of 64x32x32 ran for 1000 time-steps took approximately 30 minutes. Doubling the time-steps nearly doubled the time required to run the test.

CHAPTER VI

CONCLUSION

The behavior of plasma flow under the influence of different magnetic fields, particularly of plasma flowing through a magnetic nozzle, was examined using the lattice Boltzmann method in this thesis. Additionally, inducing detachment and the mechanism for inducing this detachment from the applied magnetic field lines was also examined. Varying certain key input parameters of the magnetic field and of the plasma produced results that agreed with theory and allowed for conclusions to be drawn. Particularly for detachment purposes it was shown that high velocities, weak magnetic fields, high fluid relaxation time, and high magnetic relaxation time can increase detachment. However, these high values also affect the ability of the magnetic field to convert thermal and gyro energy to axial energy to be used for thrust.

Validation and comparison with other computational models and physical systems was also sought. The physical system modeled in this study was that of VASIMR, which was correctly modeled qualitatively when compared to results from other computational methods. Both plasma detachment and increasing axial kinetic energy were demonstrated.

The overall mechanism for plasma detachment seemed to be a combination of both resistive and kinetic detachment. Alfvénic Mach numbers and β's above unity were seen

in the detachment case which seems to imply kinetic detachment. However the "frozen-in" condition was violated and detachment increased at higher relaxation times, which suggests resistive detachment.

Future work could seek to find ways to overcome the low Mach number limitations. Quantitative comparisons will also be sought to compare with the systems discussed in the thesis along with additional systems beyond the current qualitative results. Incorporation of additional physical features in the domain, such as a conducting wall, will also be sought to be achieved to better model VASIMR.

REFERENCES

[1] Goebel, Dan M. and Katz, Ira, *Fundamentals of Electric Propulsion*. Hoboken, NJ: Wiley, 2008.

[2] Chang Díaz, F.R., "The VASIMR Engine," *Scientific American,* Vol. 283, No. 5, 2000, pp. 72-29.

[3] Glover,T.W., Chang-Díaz F.R., et al. "Principal VASIMR Results and Present Objectives," *Space Technology and Applications International Forum*, Albuquerque, NM, 2005.

[4] Lorzel, H. and Mikillides, P.G., "Three Dimensional Modeling of Magnetic Nozzle Processes," *44th AIAA/ASME/SAE/ASEE Joint Propulsion Conference & Exhibit*, AIAA Paper 2009-4759, July 2008

[5] Riley, B. M., Girimaji, S. S., Richard, J.C., and Lee, K., "Magnetic Field Effects on Axis-Switching and Instabilities in Rectangular Plasma Jets," *Flow, Turbulence and Combustion*, Vol. 82, No. 11, 20 April 2009.

[6] Riley, B.M., "Magnetohydrodynamic Lattice Boltzmann Simulations of Turbulence and Rectangular Jet Flow," M.S. Thesis, Aerospace Engineering Dept, Texas A&M University, College Station, 2007.

[7] Deresz, Richard J.C., "Acceleration of Plasma Flow by Oscillating Magnetic Mirrors," *44th AIAA/ASME/SAE/ASEE Joint Propulsion Conference & Exhibit*, AIAA Paper 2009-4759, July 2008.

[8] Richard, J. C. and Young, B, "Multi-Species Lattice-Boltzmann Models of Xe, Xe+, Xe++, e- Flow through Ion Thruster Optics", *42nd AIAA/ASME/SAE/ASEE Joint Propulsion Conference & Exhibit* , AIAA Paper 2006-5006, July 2006.

[9] He, X., and Lou,L.-S, "Theory of the Lattice Boltzmann Method: Dispersion, Isotropy, Galilean Invariance and Stability," *Phys. Rev. E***,** Vol. 56, 6546, 2000.

[10] He, X., and Lou,L.-S, "A Priori Derivation of the Lattice Boltzmann Method: From the Boltzmann Equation to the Lattice Boltzmann Equation," *Phys Rev. E*, Vol. 61, 6811, 1997.

[11] He, X. and Luo, L.-S. "Lattice Boltzmann Model for the Incompressible Navier-Stokes Equation," *J. Stat. Phys*., Vol. 88, No ¾, 1997, pp. 926-944.

[12] Dellar, P, "Lattice Kinetic Schemes for Magnetohydrodynamics," J. Comp. Phy., Vol. 179, 95126, 2002.

[13] Matsuda, N., Kawabuchi, R., Kajimura, Y., Nakashima, H. and Zakaharov, Y.P., "Improvement of Thrust Efficiency of Laser Fusion Rocket with Shaped Target," *Journal of Physics: Conference Series*, Vol. 112, 042079, 2008.

[14] Ilin, A.V, Chang Diaz, F.R., Squire, J.P, Tarditi, A.G., Breizman, B.N., and Carter, M.D., "Simulations of Plasma Detachment in VASIMR," *40th AIAA Aerospace Sciences Meeting & Exhibit*, AIAA Paper 2002-0346, January2002.

[15] Kawabuchi, R., Matsuda, N., Kajimura, Y., Nakashima, H. and Zakaharov, Y.P., "Numerical Simulation of Plasma Detachment from a Magnetic Nozzle by Using Fully Particle-in-Cell Code," *Journal of Physics: Conference Series*, Vol. 112, 042082, 2008.

[16] Hoyt, R.P., Scheuer, J.T., Schoenberg, K.F., Gerwin, R.A., Moses, Henins, I., Black, D.C., and Mayo, R.M., "Optimization of Magnetic Nozzles for Coaxial Plasma Thrusters," *30th AIAA/ASME/SAE/ASEE Joint Propulsion Conference & Exhibit*, AIAA Paper 94-2992, June 1994.

[17] Sercel, J. C., "A Simple Model of Plasma Acceleration in a Magnetic Nozzle," AIAA 90-2597*,* 7, 1990.

[18] Arefiev, A. V. and Breizman, B. N., "Magnetohydrodynamic Scenerio of Plasma Detachment in a Magnetic Nozzle," *Physics of Plasmas* Vol. 12, 043404, 2005

[19] Breizman, B. N., Tushentsov, M.R. and Arefiev, A. V., "Magnetic Nozzle and Plasma Detachment Model for a Steady-state Flow," *Physics of Plasmas***,** Vol. 15, 057103, 2008.

[20] Deline, C., Gilchrist, B., Bengtson, R., Jones, J., Chavers, G., and Dodson, C. "Simulation and Measurement of High-Beta Plasma in a Magnetic Nozzle." *AIAA-2007-5259*, 2007.

[21] Sankaran, K. and Polzin, K. A. "Development of Numerical Tools for the Investigation of Plasma Detachment from Magnetic Nozzles." *AIAA-2007-4386*, 2007.

[22] Sankaran, K. and Polzin, K. A. "Numerical Investigation of Near-Field Plasma Flows in Magnetic Nozzles." *AIAA-2009-5358*, 2009.

[23] Chen, F, *Introduction to Plasma Physics and Controlled Fusion*, New York: Plenum Press, 1984.

[24] Hooper, E.B., "Plasma Detachment from a Magnetic Nozzle,"*Journal of Propulsion and Power*, Vol. 9, No. 5, pp. 757-763, 1993.

[25] Moses, R.W., Gerwin, R.A., and Schoenberg, R.A., "Resistive Plasma Detachment in Nozzle Based Coaxial Thrusters," *American Institue of Physics Conf. Proc.* 246, 1293 (1992).

[26] Domokos, C., and Hajagos, Imre, "Computation and Visualization of Magnetic Fields," Department of Image Processing and Computer Graphics, University of Szeged, Szeged, Hungary.

[27] Tarditi, A. G. and Shebalin, J. V., "Magnetic Nozzle Plasma Exhaust Simulation for the VASIMR Advanced Propulsion Concept," *28th International Electric Propulsion Conference*, 17-21 March 2003.

CONTACT INFORMATION

Name:	Frans Hendrik Ebersohn
Professional Address:	c/o Dr. Jacques Richard Department of Aerospace Engineering Director & Principal Investigator, NSF REU: AERO-U: Aerospace Engineering Research Opportunities for Undergraduates http://aero.tamu.edu/research/undergraduate/aero-propulsion-fluids/ College Station, TX 77843-3141, 979-845-3916 (fax 6051), http://aeweb.tamu.edu/Richard Richard@tamu.edu
Email Address:	febersohn@gmail.com
Education:	B. S. Aerospace Engineering, May 2010 Undergraduate Research Fellow Engineering Scholars Program Aerospace Honors